Multistep Kinetics of the Thermal Decomposition of β-Nickel Hydroxide: Extraction of the Primary Reaction Steps and the Effect of Water Vapor Pressure

Kazuki Arima, Yuna Kodani, Mito Hotta, and Nobuyoshi Koga*

Department of Science Education, Graduate School of Humanities and Social Sciences, Hiroshima University, 1-1-1 Kagamiyama, Higashi-Hiroshima 739-8524, Japan

Contents

* Corresponding author. e-mail: nkoga@hiroshima-u.ac.jp

S1. Sample characterization

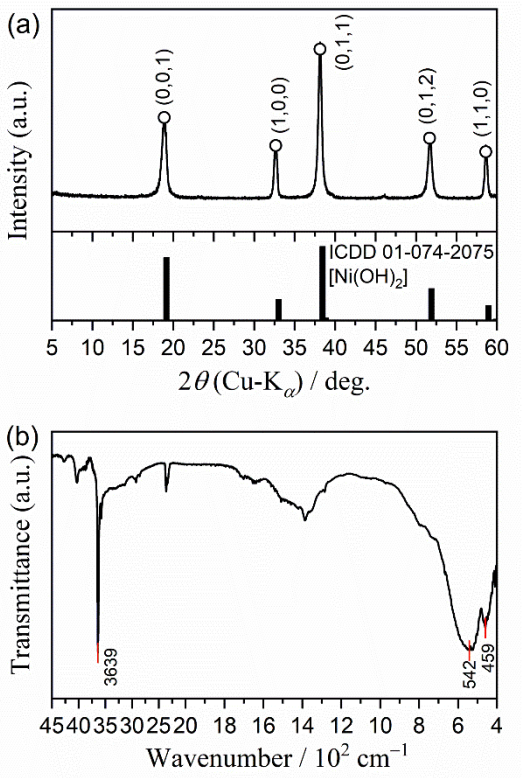

Figure S1. XRD pattern (a) and FTIR spectrum (b) of the sample.

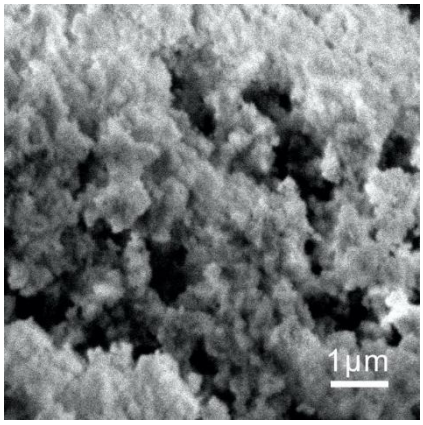

Figure S2. SEM image of the sample.

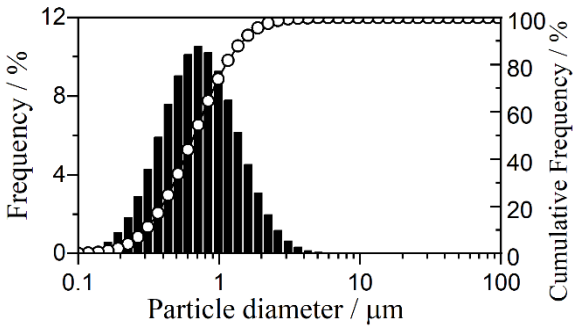

Figure S3. Particle size distribution of the sample.

S2. Thermal behavior

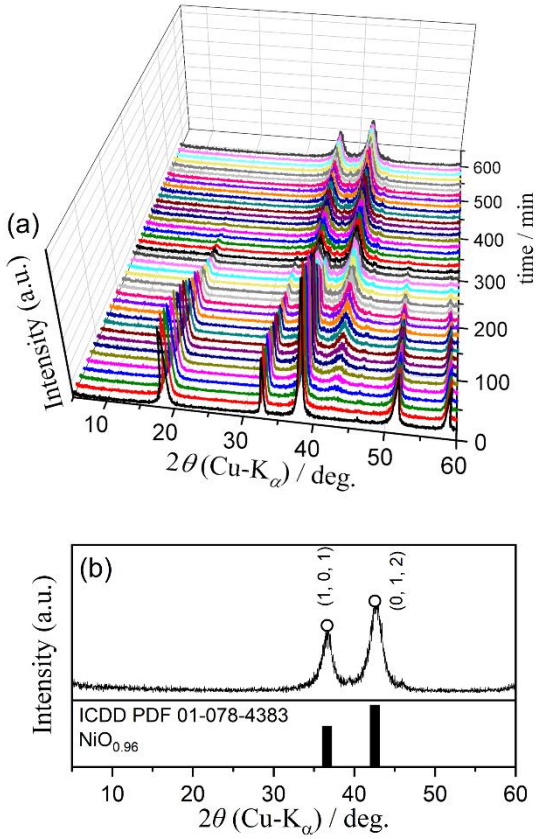

Figure S4. XRD patterns of the sample at different durations during isothermal heating at 523 K in a stream of dry N_2 (q_v = 100 cm^3 min^{-1}): (a) changes in the XRD pattern and (b) XRD pattern at 600 min duration.

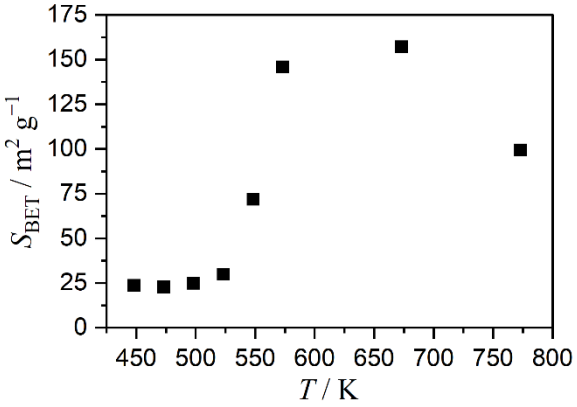

Figure S5. Variations in the S_{BET} value during the thermal decomposition of $Ni(OH)_2$ at a β of 5 K min^{-1} in a stream of dry N_2 (q_v = 100 cm^3 min^{-1}).

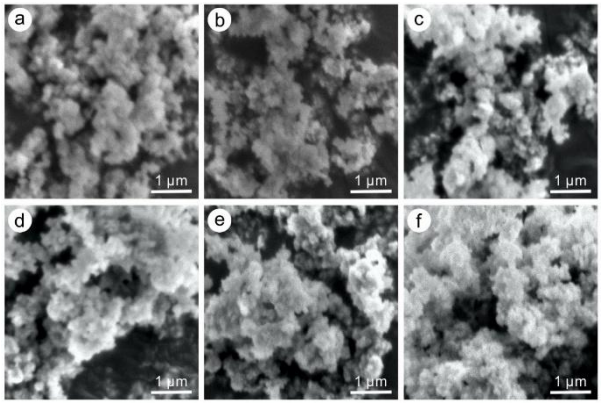

Figure S6. SEM images of the heat-treated samples obtained by heating $Ni(OH)_2$ to different temperatures at a β of 5 K min^{-1} in a stream of dry N_2 (q_v = 300 cm^3 min^{-1}): (a) original $Ni(OH)_2$, (b) 483, (c) 518, (d) 543, (e) 563, and (f) 773 K.

S3. Thermal decomposition in a stream of dry N_2

S3-1. Influence of the measurement parameters on the reaction behavior

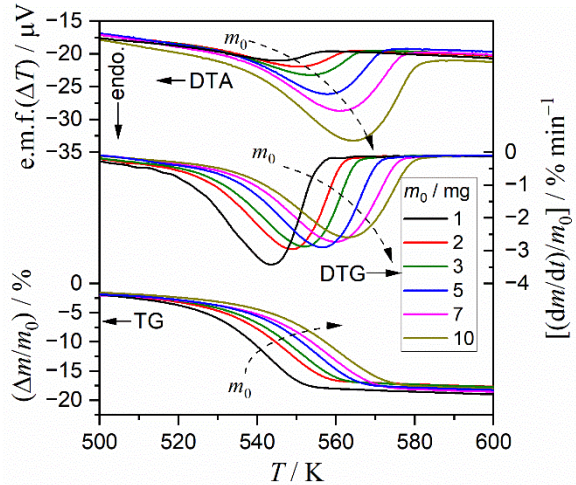

Figure S7. Variations in the TG–DTG–DTA curves for the thermal decomposition of $Ni(OH)_2$ with m_0, recorded at a β of 5 K min^{-1} in a stream of dry N_2 at a q_v of 300 cm^3 min^{-1}.

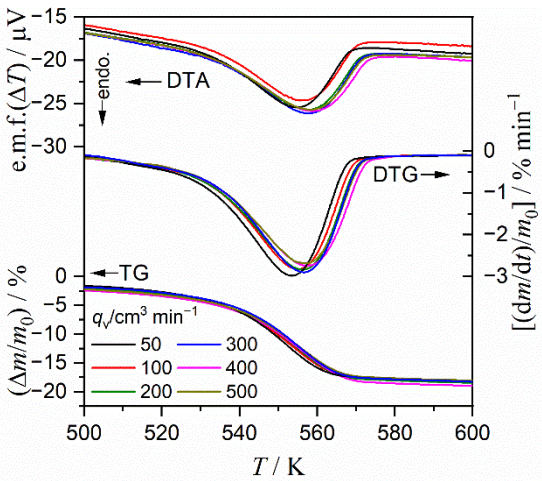

Figure S8. TG–DTG–DTA curves for the thermal decomposition of $Ni(OH)_2$ (m_0 = 5.02 ± 0.03 mg), recorded at a β of 5 K min^{-1} in a stream of dry N_2 at varying q_v values.

S3-2. Formal kinetic analysis of the overall thermal decomposition process

The isoconversional kinetic analysis has been originally based on the fundamental kinetic equation for the single-step reaction.[S1, S2]

$$\frac{d\alpha}{dt} = A\exp\left(-\frac{E_a}{RT}\right) f(\alpha), \qquad \text{(S1)}$$

where A, E_a, and R are the Arrhenius preexponential factor, apparent activation energy, and gas constant, respectively. The variation in the reaction rate as the reaction progressed at a constant temperature is described by the kinetic model function ($f(\alpha)$). The logarithmic form of eq. (S1) represents the isoconversional kinetic relationships among different series of kinetic data as the linear plot of $\ln(d\alpha/dt)$ versus T^{-1} at a given α value (Friedman plot[S3]).

$$\ln\left(\frac{d\alpha}{dt}\right) = \ln[Af(\alpha)] - \frac{E_a}{RT} \qquad \text{(S2)}$$

In the context of the ideal single-step reaction, a constant E_a value is obtained during the reaction from the slope of the Friedman plots at various α values. This is due to the constancy of the logarithmic term in the right-hand side of eq. (S2) across different series of kinetic data. However, in the case of the partially overlapping multistep process, the application of the Friedman plot results in deviations from the ideal linear correlation and apparent variation in E_a value as the reaction progressed, particularly within an α range characterized by the overlapping range of different reaction steps. While, there are some possibilities to yield a useful E_a value and its variation trend within a particular α range characterized by a component reaction step.[S4] Consequently, the Friedman plot was applied to the overall multistep mass loss process of the thermal decomposition of $Ni(OH)_2$ as a preliminary kinetic approach to identify the overlapping features of the component reaction steps and pertinent information of the individual component reaction steps.

Figure S9 shows the results of the isoconversional analysis for the overall thermal decomposition process. The statistically significant linear correlation of the Friedman plot, characterized by the correlation coefficient (γ) better than –0.99, was observed in the restricted α range of 0.10–0.74 (Figure S9(a)). A consideration of the mass loss ratios for each mass loss step indicates that the α range of 0.10–0.74 approximately corresponds to the primary mass loss process, which manifests as the second mass loss step. In the range of $\alpha <$ 0.10, corresponding to the initial mass loss step, the kinetic relationship based on eq. (S2) was not established. The initial mass loss step was anticipated as the process attributed to the desorption of absorbed or included water on the surface of and these interstices. This step exhibited less significant kinetic response to the change in the β value in the overall TG–DTG curves recorded under linear nonisothermal conditions. In the range of $\alpha > 0.74$, corresponding to the third mass loss step observed partially overlapping with the second mass loss step, the deterioration of the linear correlation of the Friedman plot as the reaction progressed and the significant fluctuation in the slope at different α values were observed. The third mass loss step was observed to be attributed to the evolution of trapped water molecules in the solid product phase induced by the crystal growth of NiO. Therefore, the evolution rate of the water vapor is the secondary trace of the crystal growth of NiO. Furthermore, the mass loss ratio during this step was limited, and the shift of the TG–DTG curve along the temperature axis in response to the change in the β values was less significant in comparison with the primary mass loss step. The observed deterioration of the linear correlation and the fluctuation of the slope may be attributed to the nature and quality of the kinetic data. The E_a values evaluated for the primary mass loss step ($0.10 \le \alpha \le 0.74$) exhibited minimal standard deviation, irrespective of α (Figure S9(b)). However, the E_a value exhibited a variation that was characterized by an initial increase from 136 kJ mol^{-1} (α = 0.10) to 141 kJ mol^{-1} (α = 0.15) and the subsequent gradual decrease to 131 kJ mol^{-1} (α = 0.74). In consideration of the partially overlapping two DTG peaks observed for the primary mass loss step under isothermal conditions, the E_a variation indicated that the primary mass loss step is composed of two reaction steps that are partially overlapping.

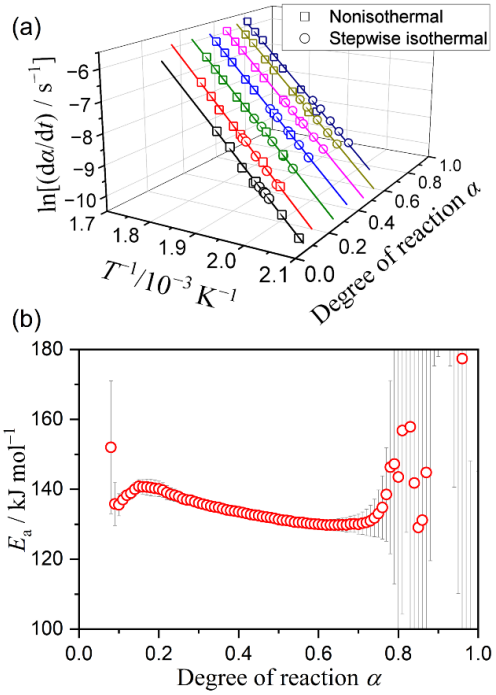

Figure S9. Results of the Friedman plots for the overall mass loss process of the thermal decomposition of $Ni(OH)_2$ in a stream of dry N_2: (a) Friedman plots at various α values ($0.10 \le \alpha \le 0.70$ in steps of 0.10) and (b) E_a values at various α values.

S3-3. Mathematical deconvolution analysis

The MDA procedure was performed using the Weibull function.

$$F(t) = a_0 \left(\frac{a_3 - 1}{a_3}\right)^{\frac{1-a_3}{a_3}} \left\{\frac{t - a_1}{a_2} + \left(\frac{a_3 - 1}{a_3}\right)^{\frac{1}{a_3}}\right\}^{a_3 - 1} \exp\left[-\left\{\frac{t - a_1}{a_2} + \left(\frac{a_3 - 1}{a_3}\right)^{\frac{1}{a_3}}\right\}^{a_3} + \frac{a_3 - 1}{a_3}\right], \quad \text{(S3)}$$

where a_0–a_3 are the parameters to express amplitude, center, width, and shape, respectively. The fitting results of the DTG curves recorded at various β values are illustrated in Figures 4 and S10.

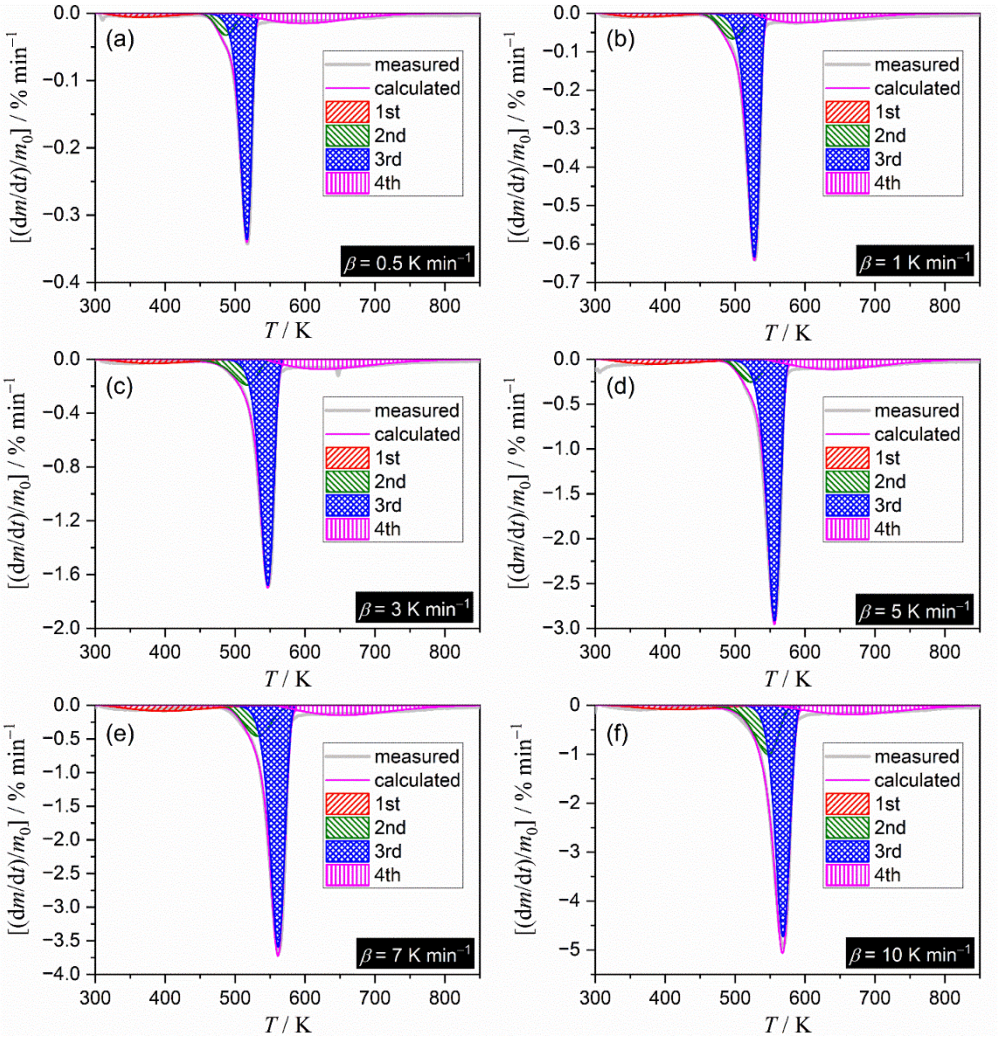

Figure S10. Fitting result of the overall DTG curves for the thermal decomposition of $Ni(OH)_2$ at various β values in a stream of dry N_2 via MDA using Weibull function: (a) 0.5, (b) 1, (c) 3, (d) 5, (e) 7, and (f) 10 K min^{-1}.

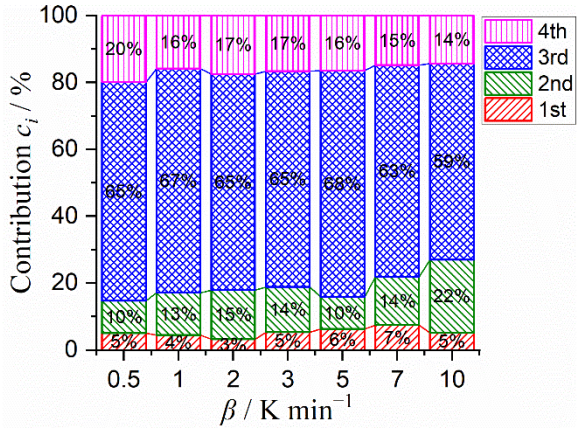

Figure S11. Contribution of each reaction steps estimated via MDA for the thermal decomposition of $Ni(OH)_2$ at various β values in a stream of dry N_2.

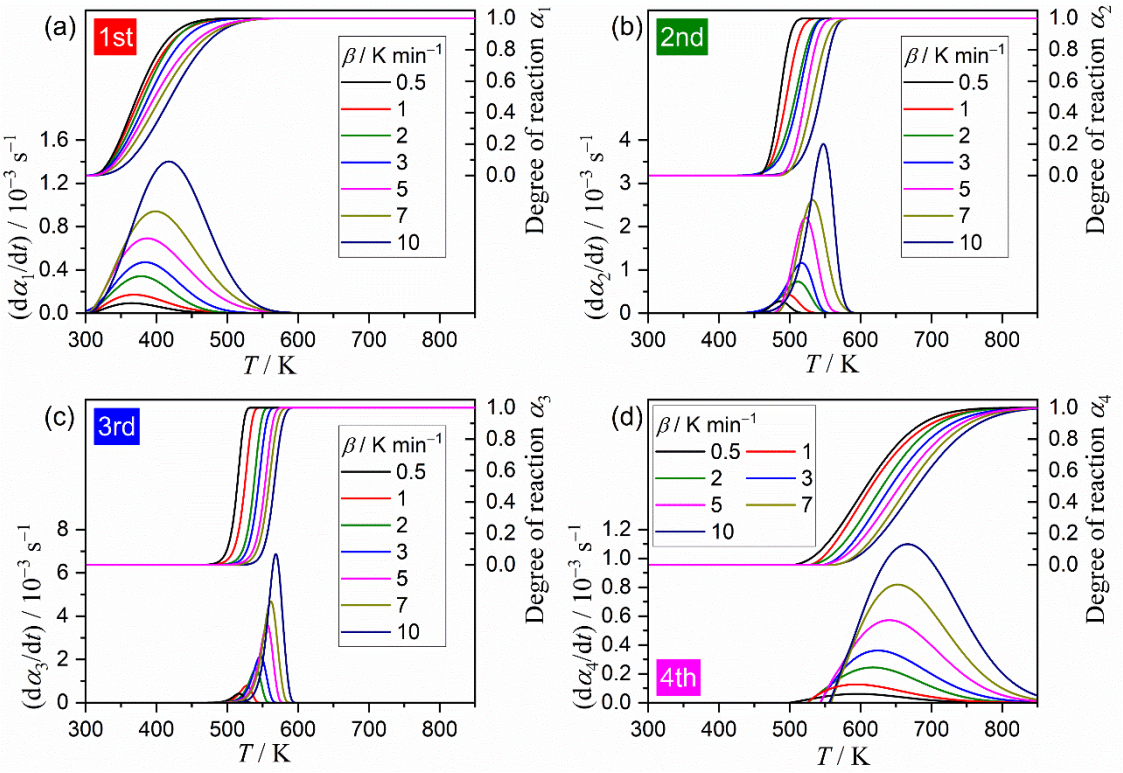

Figure S12. Kinetic data of the individual reaction steps of the thermal decomposition of $Ni(OH)_2$ at different β values, derived from the separated DTG curves via MDA: (a) first, (b) second, (c) third, and (d) fourth reaction steps.

S3-4. Formal kinetic analysis of the individual reaction steps

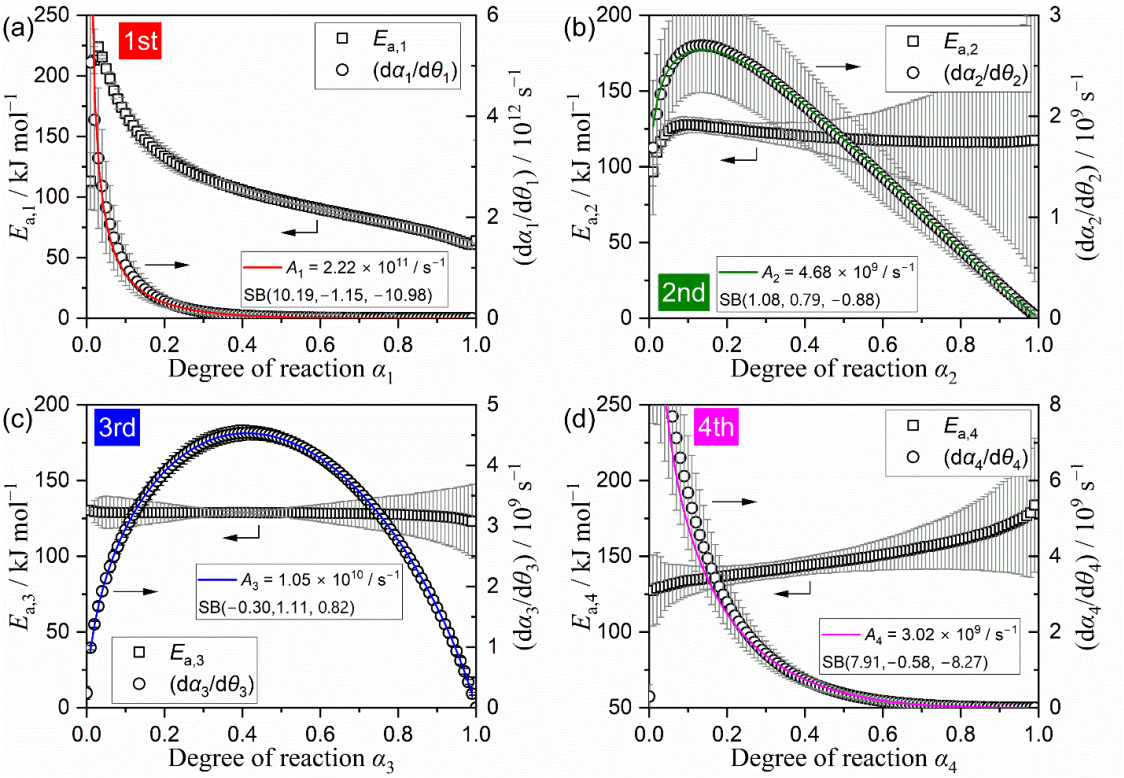

Figure S13. Results of Friedman plot and master plot analyses for the individual reaction steps of the thermal decomposition of $Ni(OH)_2$ using the kinetic data separated via MDA: (a) first, (b) second, (c) third, and (d) forth reaction steps.

Figure S13 illustrates the results of the formal kinetic analysis of the individual reaction steps of the thermal decomposition of $Ni(OH)_2$, as applied to the extracted kinetic curves under linear nonisothermal conditions via MDA (Figure S12). Initially, the series of kinetic curves of each reaction step i at different β values were subjected to the Friedman plot (eq. (S2)). The $E_{a,i}$ values ascertained by the Friedman plots at various α_i values manifested disparate variation trends as the reaction progressed. In the first reaction step, the $E_{a,1}$ value gradually decreased in conjunction with α_1. The second and third reaction steps exhibited individual constant $E_{a,2}$ and $E_{a,3}$ values during each reaction step with average values of 119.8 ± 3.7 and 128.3 ± 0.6 kJ mol^{-1} ($0.10 \leq \alpha_i \leq 0.90$), respectively. Conversely, an increasing trend of the $E_{a,4}$ value was observed for the fourth reaction step.

Assuming that each reaction step can have a constant $E_{a,i}$ value during the reaction step, the hypothetical reaction rate ($d\alpha/d\theta$) at infinite temperature was calculated at various α_i values.[S5-S9]

$$\frac{d\alpha}{d\theta} = \left(\frac{d\alpha}{dt}\right)\exp\left(\frac{E_a}{RT}\right) = Af(\alpha) \quad \text{with} \quad \theta = \int_0^t \exp\left(-\frac{E_a}{RT}\right)dt, \qquad \text{(S4)}$$

where θ is the Ozawa's generalized time, which is defined as the hypothetical reaction time at infinite temperature.[S5, S10] The experimental master plot of ($d\alpha_i/d\theta_i$) versus α_i demonstrated different forms among those in the individual reaction steps. In the first and fourth reaction steps, the experimental master plots indicated concave deceleration behaviors, while those for the second and third reaction steps exhibited a maximum reaction rate midway through each reaction step. According to eq. (S4), the individual experimental master plots were fitted using an empirical $f(\alpha)$, which is known as the Šesták–Berggren model (SB(m, n, p)),[S11-S13] and the A values for individual reaction steps were determined.

$$f(\alpha) = \alpha^m(1-\alpha)^n[-\ln(1-\alpha)]^p \qquad \text{(S5)}$$

The kinetic parameters determined through the formal kinetic analysis for the mathematically separated four reaction steps are listed in Table S1.

Table S1. Kinetic parameters for the individual reaction steps of the thermal decomposition of $Ni(OH)_2$ under linear nonisothermal conditions in a stream of dry N_2, determined from the separated kinetic data via MDA using the Friedman plot and master plot methods

Reaction step, i	Contribution, c_i [a]	$E_{a,i}$ / kJ mol^{-1} [b]	$\frac{d\alpha_i}{d\theta_i} = A_i f_i(\alpha_i)$ with SB(m_i, n_i, p_i)				
			A_i / s^{-1}	m_i	n_i	p_i	R^2 [c]
1	0.05 ± 0.01	102.5 ± 24.5	(2.22 ± 0.11) × 10^{11}	10.19 ± 0.51	–1.15 ± 0.19	–10.98 ± 0.50	0.9865
2	0.14 ± 0.04	119.8 ± 3.7	(4.68 ± 0.04) × 10^{9}	1.08 ± 0.06	0.79 ± 0.02	–0.88 ± 0.06	0.9998
3	0.64 ± 0.03	128.3 ± 0.6	(1.05 ± 0.01) × 10^{10}	–0.30 ± 0.05	1.11 ± 0.02	0.82± 0.05	0.9999
4	0.16 ± 0.02	148.3 ± 9.6	(3.02 ± 0.13) × 10^{9}	7.91 ± 0.34	–0.58 ± 0.12	–8.27 ± 0.33	0.9943

[a] Averaged over different β values.
[b] Averaged over $0.10 \leq \alpha_i \leq 0.90$.
[c] Determination coefficient of the nonlinear least-squares analysis.

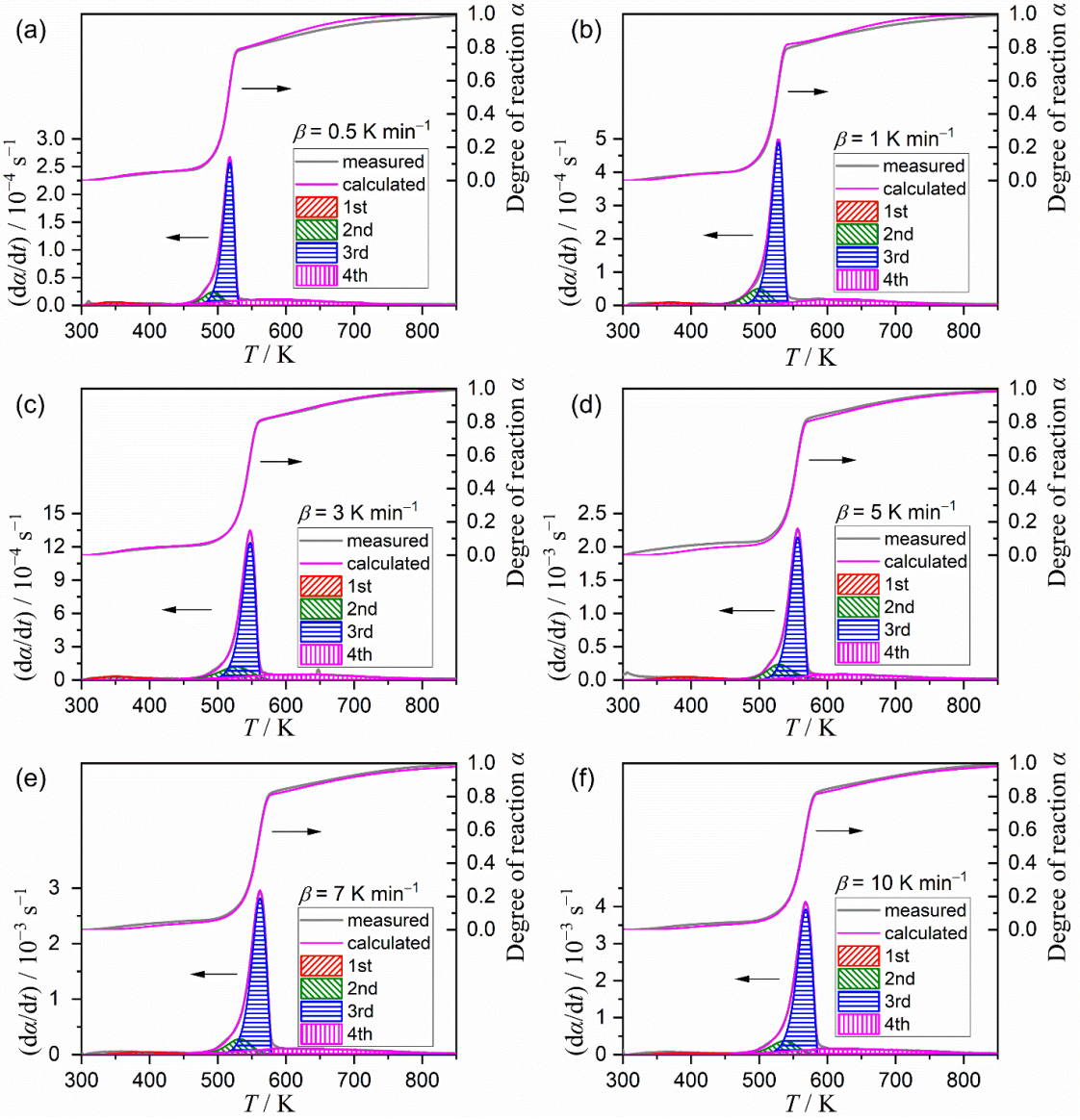

Figure S14. Results of KDA for the thermal decomposition of $Ni(OH)_2$ under linear nonisothermal conditions at different β values in a stream of dry N_2: (a) 0.5, (b) 1. (c) 3, (d) 5, (e) 7, and (f) 10 K min^{-1}.

Table S2. Average kinetic parameters for the individual reaction steps of the thermal decomposition of $Ni(OH)_2$ under linear nonisothermal conditions at different β values in a stream of dry N_2, optimized via KDA

Reaction step, i	Contribution, c_i	$E_{a,i}$ / kJ mol^{-1}	A_i / s^{-1}	SB(m_i, n_i, p_i)			$R^{2,a}$
				m_i	n_i	p_i	
1	0.05 ± 0.01	99.4 ± 4.2	(2.22 ± 0.01) × 10^{11}	10.45 ± 0.31	–1.15 ± 0.02	–10.91 ± 0.14	Diff.: 0.9990
2	0.13 ± 0.02	120.9 ± 1.0	(4.67 ± 0.02) × 10^{9}	1.15 ± 0.15	1.02 ± 0.03	–0.94 ± 0.07	Int.: 0.9996
3	0.59 ± 0.02	128.6 ± 0.3	(1.03 ± 0.03) × 10^{10}	–0.29 ± 0.04	1.00 ± 0.02	0.78± 0.03	
4	0.23 ± 0.02	152.2 ± 2.4	(3.01 ± 0.01) × 10^{9}	7.49 ± 0.33	–0.55 ± 0.05	–9.13 ± 0.32	

[a] Determination coefficient of the nonlinear least-squares analysis.

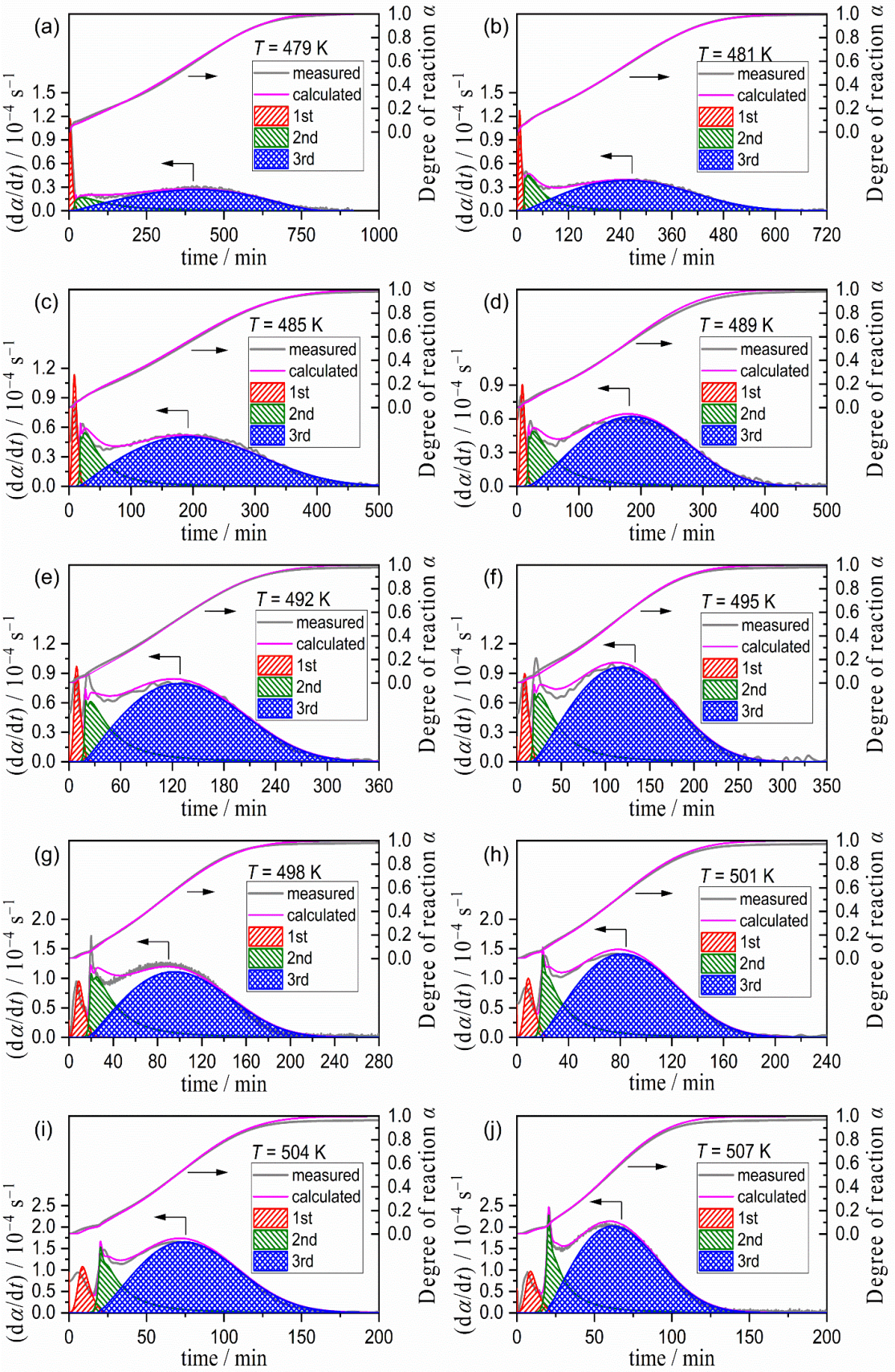

Figure S15. Results of KDA for the thermal decomposition of $Ni(OH)_2$ under isothermal conditions at different T values in a stream of dry N_2: (a) 479, (b) 481. (c) 485, (d) 489, (e) 492, (f) 495, (g) 498, (h) 501, (i) 504, and (j) 507 K.

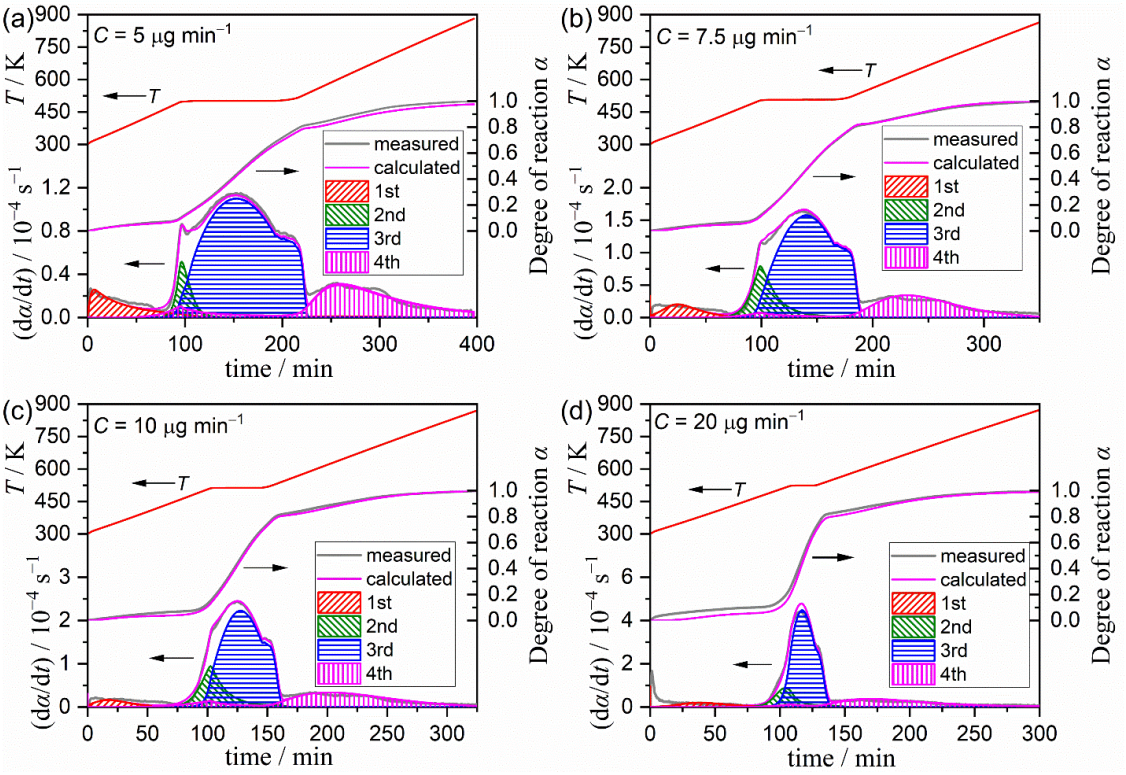

Figure S16. Results of KDA for the thermal decomposition of $Ni(OH)_2$ under stepwise isothermal conditions at different *C* values in a stream of dry N_2: (a) 5, (b) 7.5. (c) 10, and (d) 20 μg min^{-1}.

Table S3. Average kinetic parameters for the individual reaction steps of the thermal decomposition of $Ni(OH)_2$ under isothermal conditions at different T values in a stream of dry N_2, optimized via KDA

Reaction step, i	Contribution, c_i	$E_{a,i}$ / kJ mol^{-1}	A_i / s^{-1}	SB(m_i, n_i, p_i)			$R^{2,a}$
				m_i	n_i	p_i	
1	0.06 ± 0.01	96.4 ± 5.7	(2.05 ± 0.55) × 10^{11}	11.21 ± 2.22	–1.33 ± 0.58	–11.63 ± 2.13	Diff: 0.9665
2	0.18 ± 0.01	120.6 ± 1.0	(4.67 ± 0.01) × 10^{9}	1.12 ± 0.03	1.03 ± 0.01	–0.97 ± 0.03	Int: 0.9991
3	0.77 ± 0.01	128.8 ± 0.4	(1.03 ± 0.01) × 10^{10}	–0.30 ± 0.01	1.00 ± 0.06	0.81± 0.01	

[a] Determination coefficient of the nonlinear least-squares analysis.

Table S4. Average kinetic parameters for the individual reaction steps of the thermal decomposition of $Ni(OH)_2$ under stepwise isothermal conditions at different C values in a stream of dry N_2, optimized via KDA

Reaction step, i	Contribution, c_i	$E_{a,i}$ / kJ mol^{-1}	A_i / s^{-1}	SB(m_i, n_i, p_i)			$R^{2,a}$
				m_i	n_i	p_i	
1	0.05 ± 0.02	91.9 ± 2.8	(2.73 ± 1.01) × 10^{11}	13.36 ± 5.87	–0.97 ± 0.40	–13.54 ± 5.67	Diff.: 0.9983
2	0.12 ± 0.04	120.3 ± 2.7	(4.65 ± 0.02) × 10^{9}	1.16 ± 0.18	0.94 ± 0.28	–0.94 ± 0.07	Int.: 0.9997
3	0.60 ± 0.02	128.8 ± 0.2	(9.85 ± 0.49) × 10^{9}	–0.31 ± 0.01	0.95 ± 0.03	0.79 ± 0.03	
4	0.23 ± 0.02	152.1 ± 3.7	(3.01 ± 0.01) × 10^{9}	8.68 ± 2.64	–0.54 ± 0.06	–10.51 ± 2.33	

[a] Determination coefficient of the nonlinear least-squares analysis.

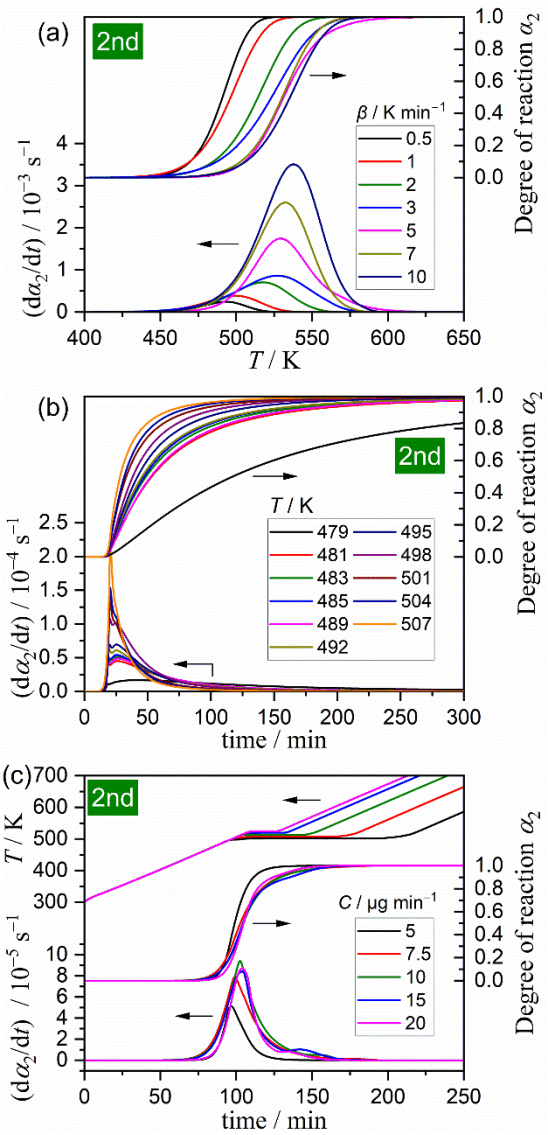

Figure S17. Extracted kinetic curves for the second reaction step of the thermal decomposition of $Ni(OH)_2$ under different heating conditions in a stream of dry N_2: (a) linear nonisothermal, (b) isothermal, and (c) stepwise isothermal conditions.

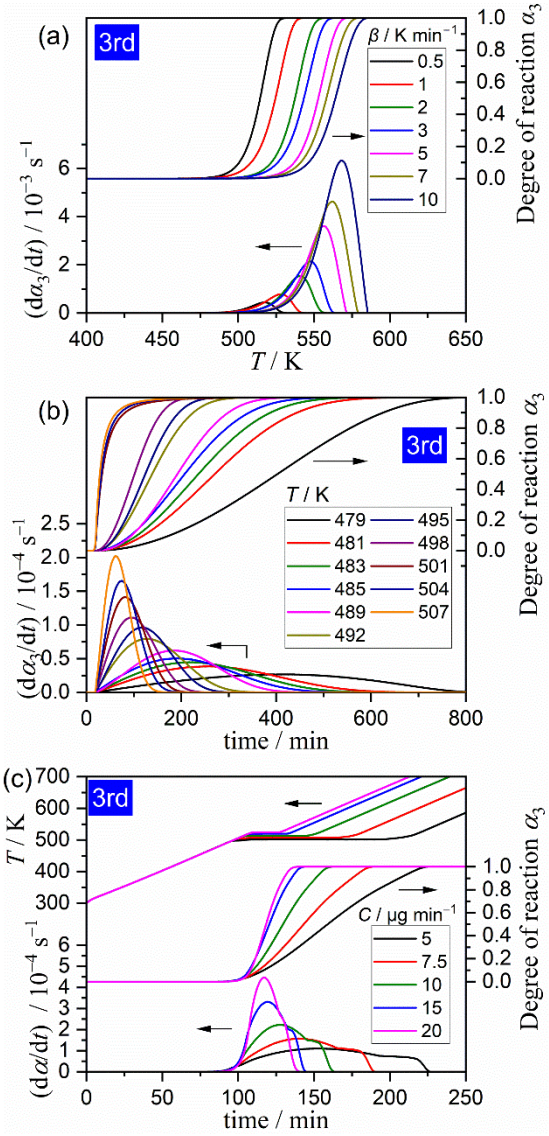

Figure S18. Extracted kinetic curves for the third reaction step of the thermal decomposition of $Ni(OH)_2$ under different heating conditions in a stream of dry N_2: (a) linear nonisothermal, (b) isothermal, and (c) stepwise isothermal conditions.

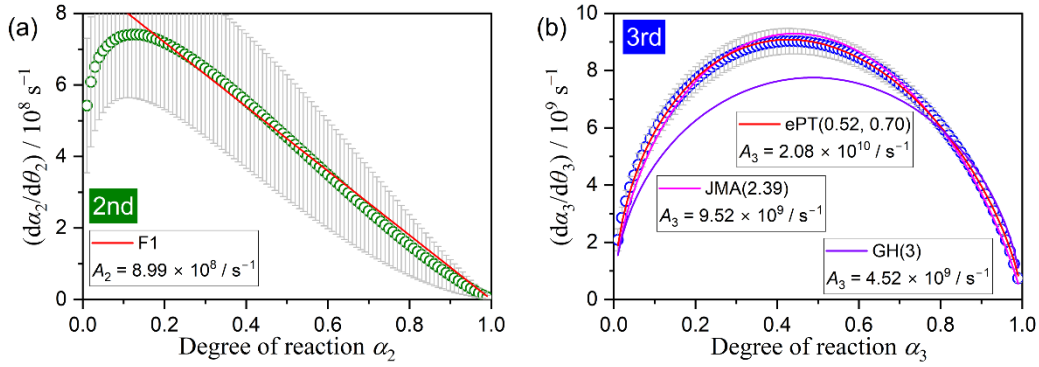

Figure S19. Analyses of the experimental master plots of the individual reaction steps of the thermal decomposition of $Ni(OH)_2$ using physico-chemical and physico-geometrical kinetic model functions: (a) second and (b) third reaction steps.

S4. Thermal decomposition in a stream of wet N_2 with various atmospheric water vapor pressures

S4-1. Kinetic curves and formal kinetic analysis of the overall reaction process

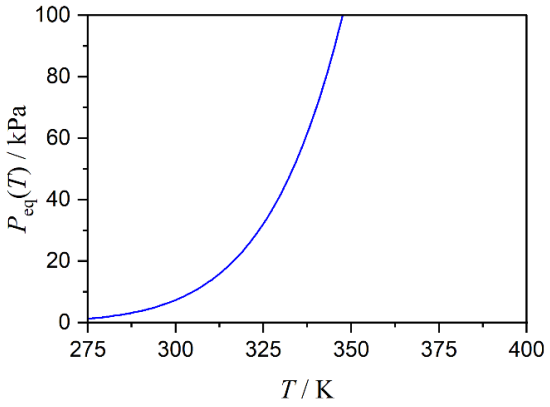

Figure S20. Equilibrium water vapor pressure ($P_{eq}(T)$) of the thermal decomposition of $Ni(OH)_2$ at varying temperatures. The $P_{eq}(T)$ values were calculated using the available literature values of the thermodynamic parameters of the component materials of the reaction system,[S14] while the specific heat capacity of $Ni(OH)_2$ was determined to be 99.6 J $(mol \cdot K)^{-1}$ using differential scanning calorimetry with reference to the specific heat capacity of α-Al_2O_3.

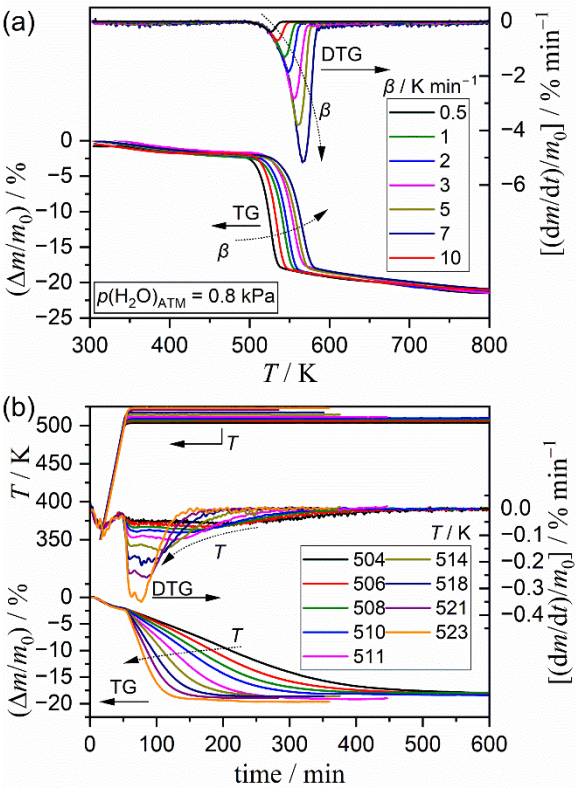

Figure S21. TG–DTG curves for the thermal decomposition of $Ni(OH)_2$ under different heating conditions in a stream of wet N_2 characterized by $p(H_2O)_{ATM}$ = 0.8 ± 0.1 kPa: (a) linear nonisothermal conditions at various β values (m_0 = 5.01 ± 0.03 mg) and (b) isothermal conditions at various T values (m_0 = 5.00 ± 0.02 mg).

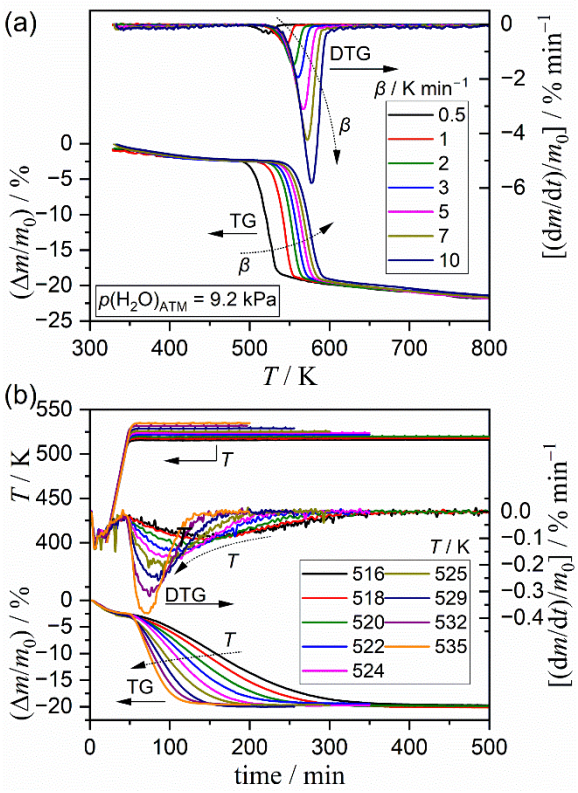

Figure S22. TG–DTG curves for the thermal decomposition of $Ni(OH)_2$ under different heating conditions in a stream of wet N_2 characterized by $p(H_2O)_{ATM}$ = 9.2 ± 0.2 kPa: (a) linear nonisothermal conditions at various β values (m_0 = 5.02 ± 0.02 mg) and (b) isothermal conditions at various T values (m_0 = 5.01 ± 0.02 mg).

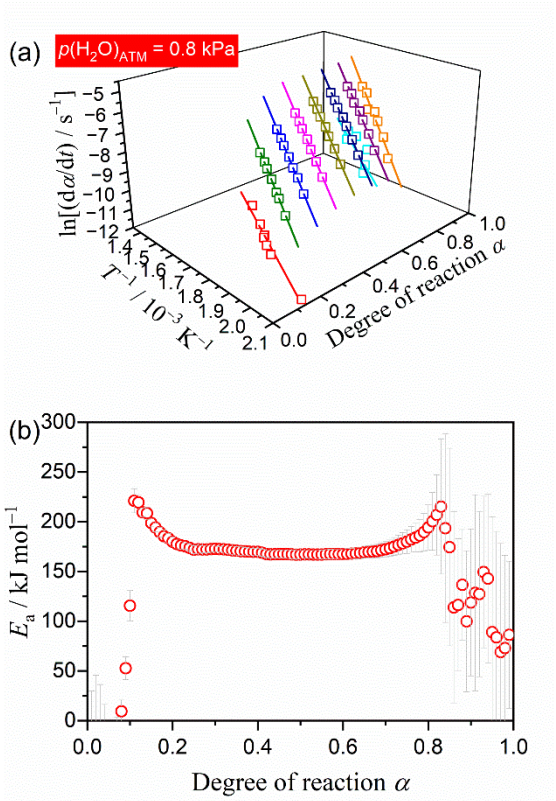

Figure S23. Friedman plots for the overall process of the thermal decomposition of $Ni(OH)_2$ in a stream of wet N_2 with $p(H_2O)_{ATM}$ = 0.8 kPa (a) Friedman plots at various α values and (b) E_a values at various α values.

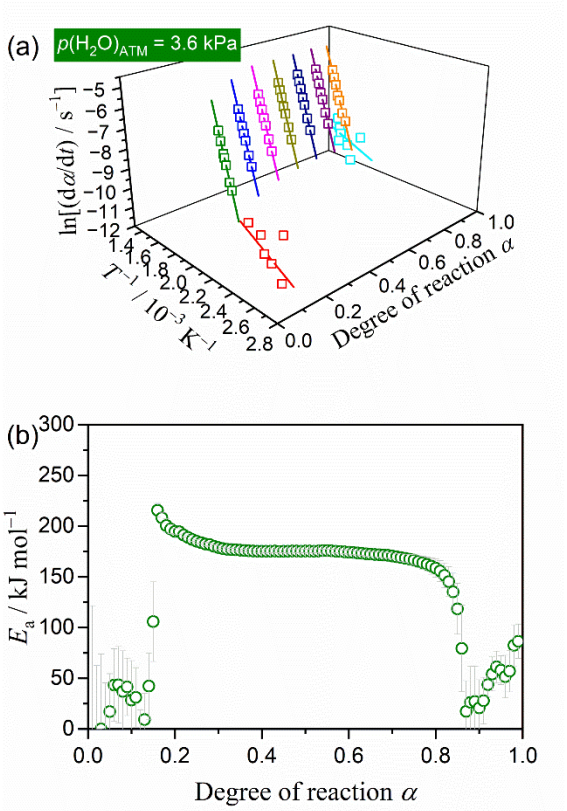

Figure S24. Friedman plots for the overall process of the thermal decomposition of $Ni(OH)_2$ in a stream of wet N_2 with $p(H_2O)_{ATM}$ = 3.6 kPa: (a) Friedman plots at various α values and (b) E_a values at various α values.

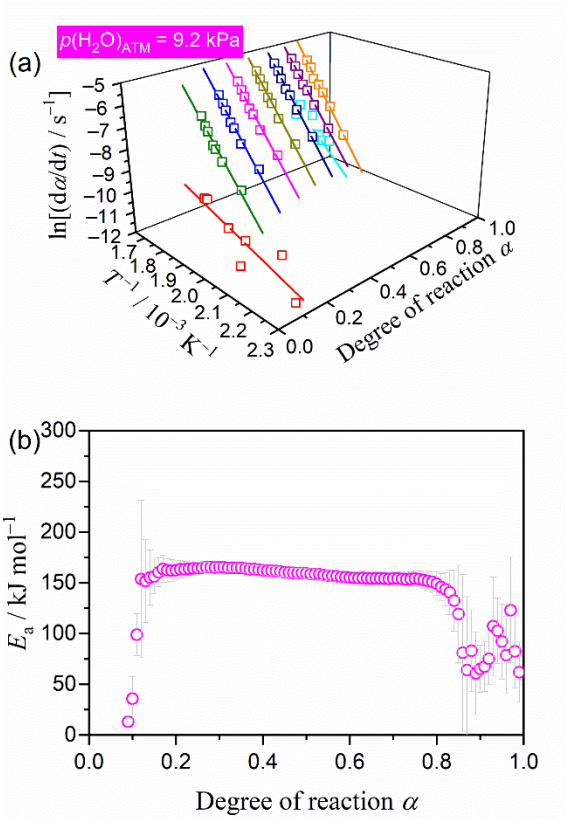

Figure S25. Friedman plots for the overall process of the thermal decomposition of $Ni(OH)_2$ in a stream of wet N_2 with $p(H_2O)_{ATM}$ = 9.2 kPa: (a) Friedman plots at various α values and (b) E_a values at various α values.

S4-2. Deconvolution of the multistep reaction process

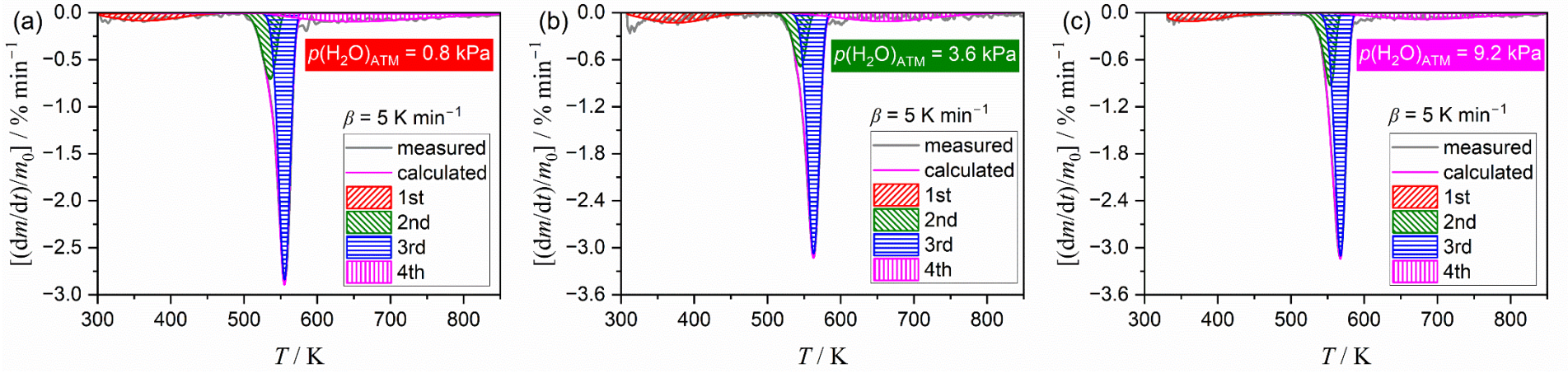

Figure S26. Typical results of MDA for the thermal decomposition of $Ni(OH)_2$ under linear nonisothermal conditions at a β of 5 K min^{-1} in a stream of wet N_2 characterized by varying $p(H_2O)_{ATM}$ values: (a) 0.8, (b) 3.6, and (c) 9.2 kPa.

Table S5. Kinetic parameters for the individual reaction steps of the primary reaction process of the thermal decomposition of $Ni(OH)_2$ under linear nonisothermal conditions in a stream of wet N_2 with different $p(H_2O)$ values, determined from the separated kinetic data via MDA using the Friedman plot and master plot methods

Reaction step, i	$p(H_2O)$ / kPa	$c_i/(c_2+c_3)$ [a]	$E_{a,i}$ / kJ mol^{-1} [b]	$\frac{d\alpha_i}{dt} = A_i f_i(\alpha_i)$ with $f_i(\alpha_i) = \alpha_i^{m_i}(1-\alpha_i)^{n_i}[-\ln(1-\alpha_i)]^{p_i}$				
				A_i / s^{-1}	m_i	n_i	p_i	R^2 [c]
2	0.8	0.22 ± 0.04	171.8 ± 7.3	(4.23 ± 0.02) × 10^{14}	0.61 ± 0.05	0.87 ± 0.02	–0.27 ± 0.04	0.9999
	3.6	0.18 ± 0.04	188.2 ± 2.3	(9.74 ± 0.08) × 10^{15}	1.26 ± 0.08	0.69 ± 0.03	–0.91 ± 0.08	0.9997
	9.2	0.22 ± 0.04	178.1 ± 6.2	(5.85 ± 0.02) × 10^{14}	–0.32 ± 0.03	1.08 ± 0.01	0.70 ± 0.03	0.9999
3	0.8	0.78 ± 0.04	170.9 ± 2.4	(1.21 ± 0.01) × 10^{14}	0.35 ± 0.01	0.97 ± 0.01	0.16 ± 0.01	0.9999
	3.6	0.82 ± 0.04	183.0 ± 0.8	(9.92 ± 0.01) × 10^{14}	0.23 ± 0.01	1.00 ± 0.01	0.25 ± 0.01	0.9999
	9.2	0.78 ± 0.04	160.5 ± 7.5	(6.64 ± 0.01) × 10^{12}	0.38 ± 0.02	0.95 ± 0.01	0.18 ± 0.02	0.9999

[a] Averaged over different β values.
[b] Averaged over $0.10 \le \alpha \le 0.90$.
[c] Determination coefficient of the nonlinear least-squares analysis.

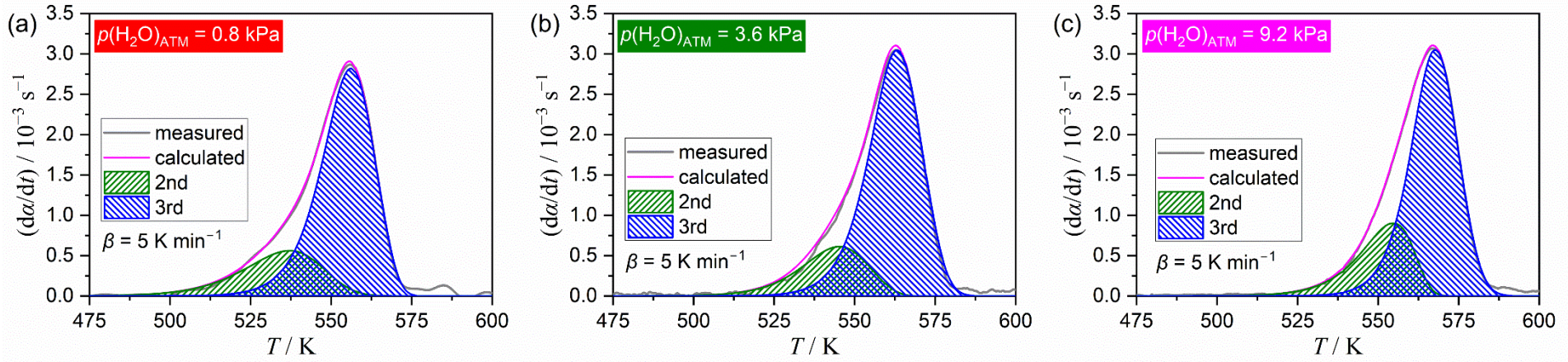

Figure S27. Typical results of KDA for the primary process of the thermal decomposition of $Ni(OH)_2$ under linear nonisothermal conditions at a β of 5 K min^{-1} in a stream of wet N_2 characterized by varying $p(H_2O)_{ATM}$ values: (a) 0.8, (b) 3.6, and (c) 9.2 kPa.

Table S6. Average kinetic parameters for the individual reaction steps of the primary reaction process of the thermal decomposition of $Ni(OH)_2$ under linear nonisothermal conditions at varying β values in a stream of wet N_2 with different $p(H_2O)_{ATM}$ values, optimized through KDA

Reaction step, i	$p(H_2O)_{ATM}$ / kPa	$c_i/(c_2+c_3)$	$E_{a,i}$ / kJ mol^{-1}	A_i / s^{-1}	SB(m_i, n_i, p_i)			$R^{2,a}$
					m_i	n_i	p_i	
2	0.8	0.23 ± 0.04	172.7 ± 0.7	(4.21 ± 0.02) × 10^{14}	0.55 ± 0.07	0.84 ± 0.08	–0.28 ± 0.02	0.9980
	3.6	0.18 ± 0.04	188.8 ± 1.5	(9.73 ± 0.03) × 10^{15}	1.16 ± 0.13	0.65 ± 0.12	–0.95 ± 0.08	0.9936
	9.2	0.24 ± 0.04	179.0 ± 0.7	(5.84 ± 0.02) × 10^{14}	–0.34 ± 0.03	0.99 ± 0.13	0.66 ± 0.08	0.9980
3	0.8	0.77 ± 0.04	170.6 ± 0.8	(1.18 ± 0.06) × 10^{14}	0.39 ± 0.04	0.99 ± 0.08	0.17 ± 0.02	0.9980
	3.6	0.82 ± 0.04	182.7 ± 0.8	(9.59 ± 0.68) × 10^{14}	0.24 ± 0.01	1.08 ± 0.05	0.27± 0.03	0.9936
	9.2	0.76 ± 0.04	160.0 ± 0.7	(6.57 ± 0.14) × 10^{12}	0.45 ± 0.04	1.03 ± 0.01	0.20 ± 0.01	0.9980

[a] Determination coefficient of the nonlinear least-squares analysis.

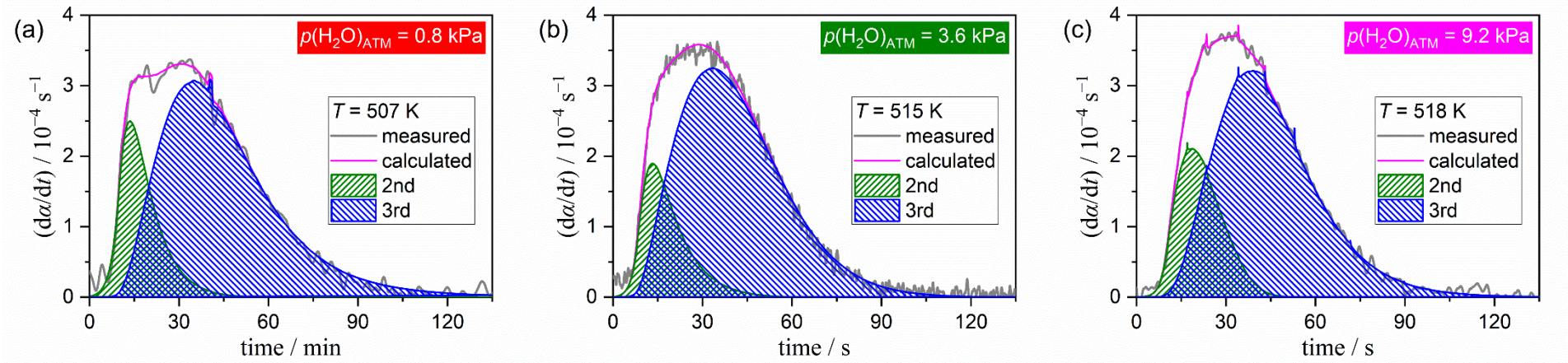

Figure S28. Typical results of KDA for the primary process of the thermal decomposition of $Ni(OH)_2$ under isothermal conditions at a temperature in a stream of wet N_2 characterized by varying $p(H_2O)_{ATM}$ values: (a) 0.8, (b) 3.6, and (c) 9.2 kPa.

Table S7. Average kinetic parameters for the individual reaction steps of the primary reaction process of the thermal decomposition of $Ni(OH)_2$ under isothermal conditions at varying T values in a stream of wet N_2 with different $p(H_2O)_{ATM}$ values, optimized through KDA

Reaction step, i	$p(H_2O)_{ATM}$ / kPa	$c_i/(c_2+c_3)$	$E_{a,i}$ / kJ mol^{-1}	A_i / s^{-1}	SB(m_i, n_i, p_i)			$R^{2,a}$
					m_i	n_i	p_i	
2	0.8	0.22 ± 0.01	173.3 ± 0.5	(4.21 ± 0.01) × 10^{14}	0.54 ± 0.02	0.85 ± 0.02	–0.28 ± 0.02	0.9420
	3.6	0.18 ± 0.01	191.2 ± 1.0	(9.72 ± 0.01) × 10^{15}	1.15 ± 0.03	0.65 ± 0.01	–0.96 ± 0.02	0.9876
	9.2	0.24 ± 0.01	179.9 ± 0.3	(5.84 ± 0.01) × 10^{14}	–0.33 ± 0.03	0.99 ± 0.01	0.66 ± 0.01	0.9881
3	0.8	0.78 ± 0.01	171.5 ± 0.7	(1.18 ± 0.07) × 10^{14}	0.40 ± 0.02	1.01 ± 0.06	0.17 ± 0.01	0.9420
	3.6	0.82 ± 0.01	183.2 ± 0.2	(9.58 ± 0.01) × 10^{14}	0.24 ± 0.01	1.02 ± 0.05	0.28 ± 0.01	0.9876
	9.2	0.76 ± 0.01	161.2 ± 0.2	(6.57 ± 0.01) × 10^{12}	0.44 ± 0.01	1.04 ± 0.01	0.19 ± 0.01	0.9881

[a] Determination coefficient of the nonlinear least-squares analysis.

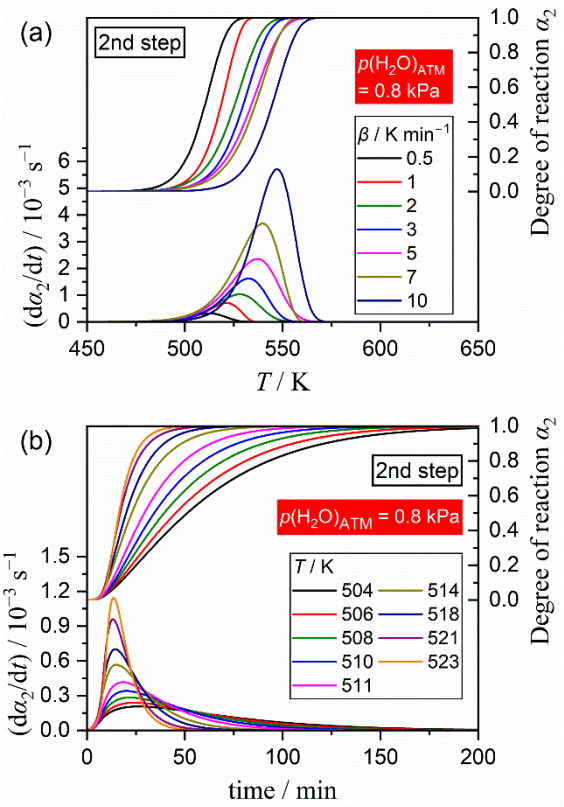

Figure S29. Kinetic data for the second reaction step of the thermal decomposition of $Ni(OH)_2$ under (a) linear nonisothermal and (b) isothermal conditions in a stream of wet N_2 with a $p(H_2O)_{ATM}$ of 0.8 kPa.

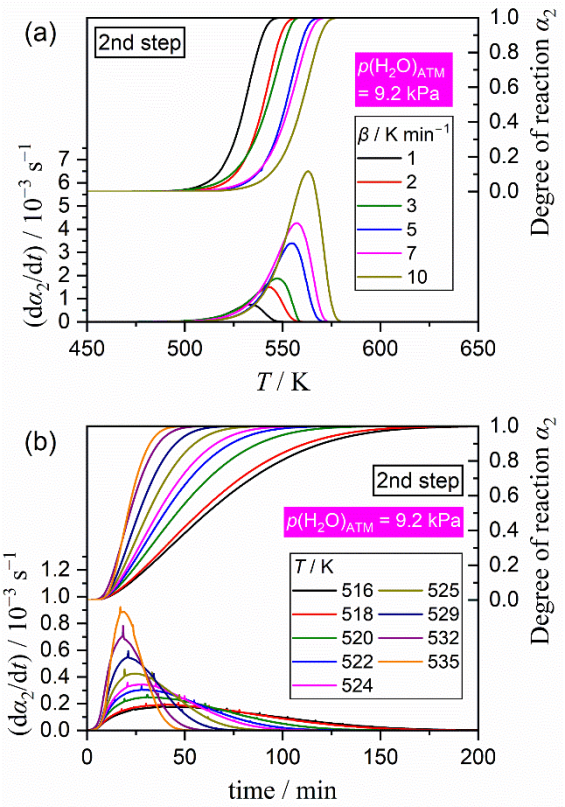

Figure S31. Kinetic data for the second reaction step of the thermal decomposition of $Ni(OH)_2$ under (a) linear nonisothermal and (b) isothermal conditions in a stream of wet N_2 with a $p(H_2O)_{ATM}$ of 9.2 kPa.

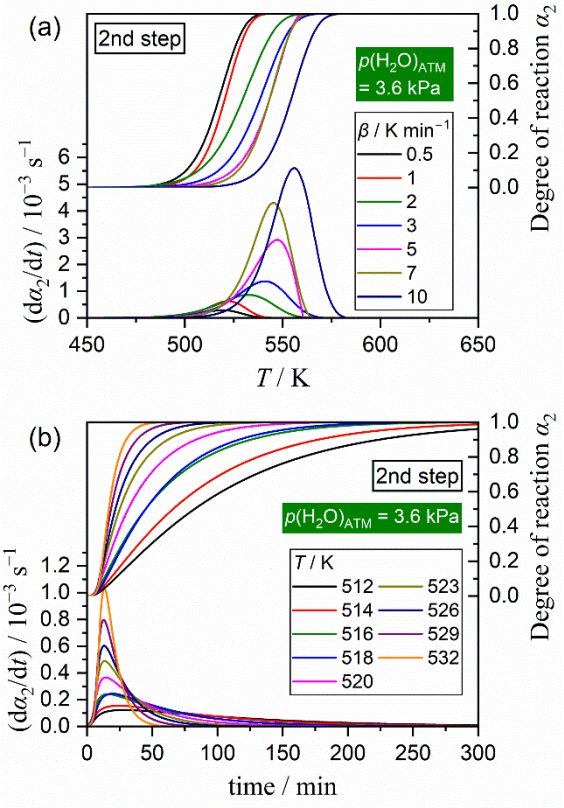

Figure S30. Kinetic data for the second reaction step of the thermal decomposition of $Ni(OH)_2$ under (a) linear nonisothermal and (b) isothermal conditions in a stream of wet N_2 with a $p(H_2O)_{ATM}$ of 3.6 kPa.

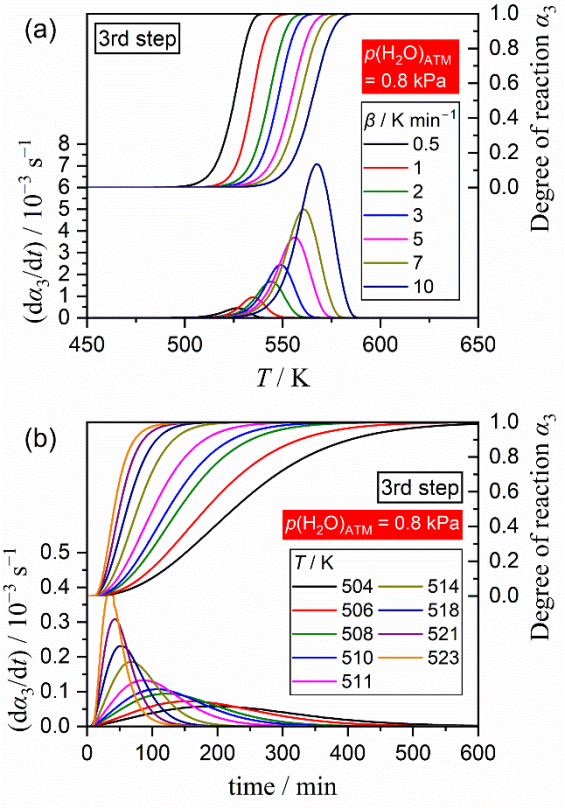

Figure S32. Kinetic data for the third reaction step of the thermal decomposition of $Ni(OH)_2$ under (a) linear nonisothermal and (b) isothermal conditions in a stream of wet N_2 with a $p(H_2O)_{ATM}$ of 0.8 kPa.

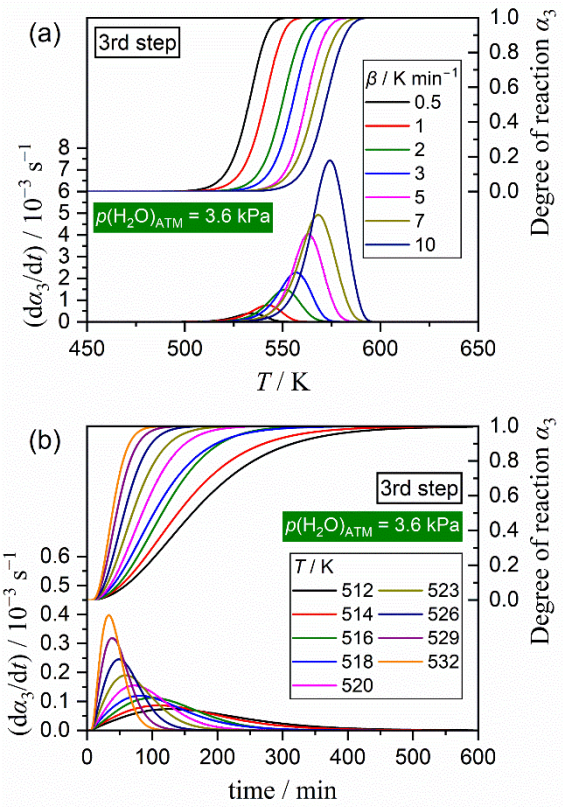

Figure S33. Kinetic data for the third reaction step of the thermal decomposition of $Ni(OH)_2$ under (a) linear nonisothermal and (b) isothermal conditions in a stream of wet N_2 with a $p(H_2O)_{ATM}$ of 3.6 kPa.

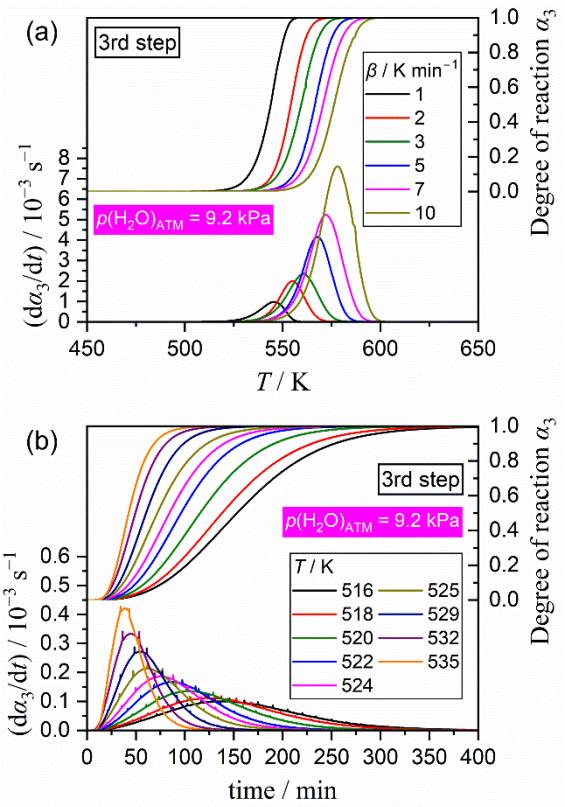

Figure S34. Kinetic data for the third reaction step of the thermal decomposition of $Ni(OH)_2$ under (a) linear nonisothermal and (b) isothermal conditions in a stream of wet N_2 with a $p(H_2O)_{ATM}$ of 9.2 kPa.

S4-3. Formal kinetic analysis for the primary reaction process by ignoring the effect of $p(H_2O)$

The extracted kinetic data of the second and third reaction steps under linear nonisothermal and isothermal conditions at each $p(H_2O)_{ATM}$ value were simultaneously subjected to the formal kinetic analysis by ignoring the effect of $p(H_2O)$. The kinetic results for the second reaction step are illustrated in Figures S35 and S36, and the yielded kinetic parameters are summarized in Table S8. At each $p(H_2O)_{ATM}$ value, the Friedman plot exhibited a statistically significant linear correlation at individual α_2 (Figure S35). However, distinct linear correlations were observed among different $p(H_2O)_{ATM}$ values (Figure S36(a)). The yielded $E_{a,2}$ values at specific α_2 values and the variation trends as the reaction progressed exhibited differences among reactions at varying $p(H_2O)_{ATM}$ values (Figure S36(b)). Furthermore, the experimental master plots demonstrated varied shapes among the reactions at different $p(H_2O)_{ATM}$ values and exhibited irregular variations with the alteration in the $p(H_2O)_{ATM}$ value (Figure S36(c)). The apparent kinetic parameters determined by ignoring the effect of $p(H_2O)$ exhibited distinct values among the reactions at different $p(H_2O)_{ATM}$ values (Table S8).

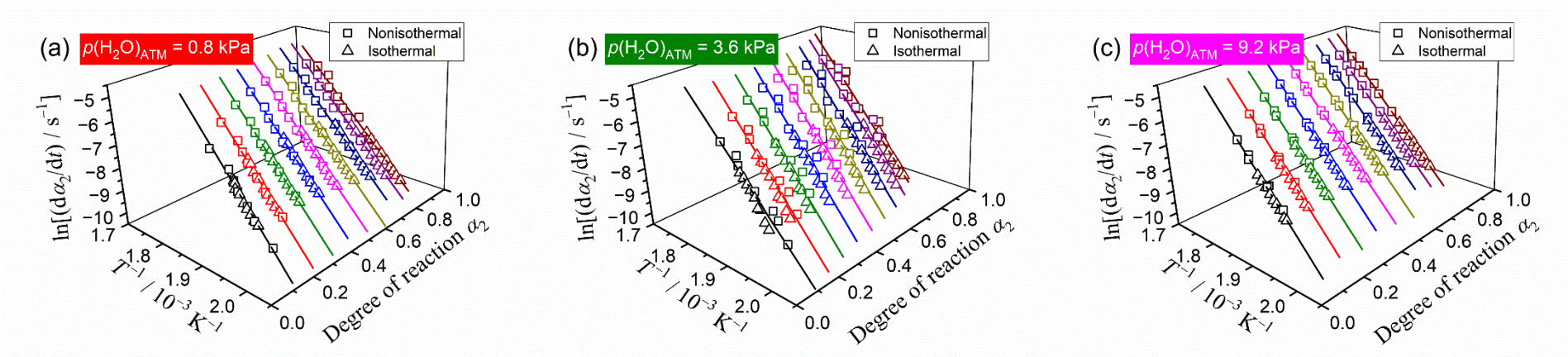

Figure S35. Friedman plots for the second reaction step of the thermal decomposition of $Ni(OH)_2$ under linear nonisothermal and isothermal conditions in a stream of wet N_2 with varying $p(H_2O)_{ATM}$ values: (a) 0.8, (b) 3.6, and (c) 9.2 kPa.

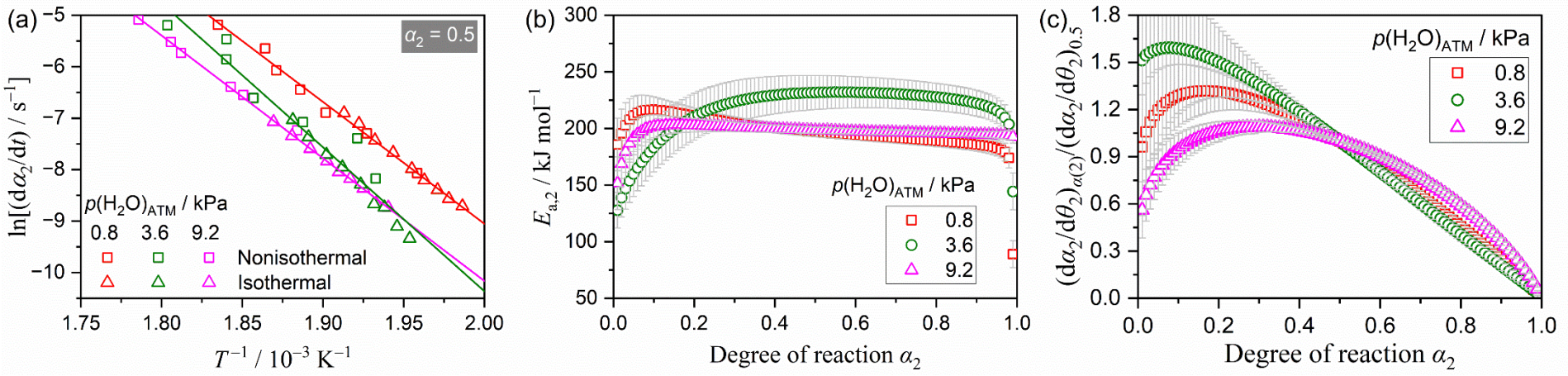

Figure S36. Comparison of the results of formal kinetic analysis for the second reaction step of the thermal decomposition of $Ni(OH)_2$ at different $p(H_2O)_{ATM}$ values: (a) Friedman plots at $\alpha_2 = 0.5$, (b) variation of $E_{a,2}$ value as the reaction progressed, and (c) normalized experimental master plot.

Table S8. Kinetic parameters for the second reaction step of the thermal decomposition of $Ni(OH)_2$ at individual $p(H_2O)_{ATM}$ values, determined by the formal kinetic analysis via Friedman plot and experimental master plot methods

$p(H_2O)_{ATM}$ / kPa	$E_{a,2}$ / kJ mol^{-1}, [a]	$\frac{d\alpha_2}{d\theta_2} = A_2 f_2(\alpha_2)$ with $f_2(\alpha_2) = \alpha_2^{m_2}(1-\alpha_2)^{n_2}[-\ln(1-\alpha_2)]^{p_2}$				
		A_2 / s^{-1}	m_2	n_2	p_2	$R^{2,b}$
0.8	198.7 ± 8.9	(1.61 ± 0.01) × 10^{17}	0.55 ± 0.04	0.81 ± 0.02	–0.35 ± 0.04	0.9999
3.6	223.7 ± 11.6	(2.12 ± 0.02) × 10^{19}	1.49 ± 0.05	0.50 ± 0.02	–1.37 ± 0.05	0.9998
9.2	198.8 ± 2.7	(4.39 ± 0.01) × 10^{16}	–0.34 ± 0.02	0.97 ± 0.01	0.62 ± 0.02	0.9999

[a] Averaged over $0.10 \le \alpha_2 \le 0.90$.
[b] Determination coefficient of the nonlinear least-squares analysis.

The kinetic results for the third reaction steps are depicted in Figures S37, S38, and Table S9. Irrespective of $p(H_2O)_{ATM}$ value, the Friedman plots exhibited an excellent linear correlation and constant slope during the third reaction step (Figure S37). The Friedman plot exhibited a parallel shift accompanied by an increase in the $p(H_2O)_{ATM}$ value from 0.8 to 3.6 kPa and a slight decline with that from 3.6 to 9.2 kPa (Figure S38(a)). Consequently, the $E_{a,3}$ values for the reactions at 0.8 and 3.6 kPa were approximately identical during the third reaction step (Figure S38(b)), while the slightly smaller $E_{a,3}$ values were estimated for the reaction at 9.2 kPa. Regardless of the variation in $E_{a,3}$ value with $p(H_2O)_{ATM}$, the shape of the experimental master plot remained independent of the $p(H_2O)_{ATM}$ value (Figure S38(c)). The variation in the kinetic behavior with the increase in the $p(H_2O)$ value from 0.8 to 3.6 kPa was characterized by the decrease in the A_3 value, while the $E_{a,3}$ value remained constant (Table S9). In contrast, the variation associated with the increase in the $p(H_2O)_{ATM}$ value from 3.6 to 9.2 kPa was characterized by the decline of both $E_{a,3}$ and A_3 values.

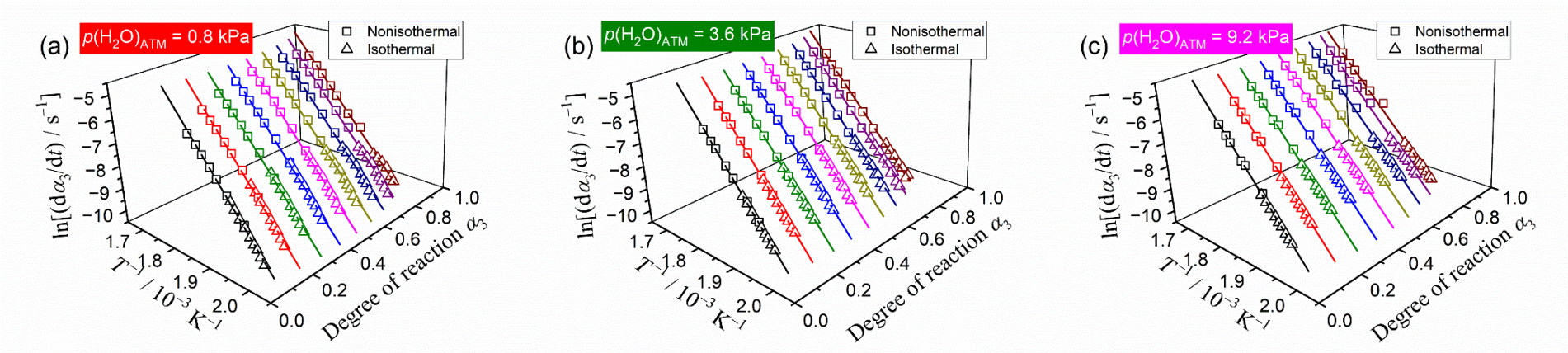

Figure S37. Friedman plots for the third reaction step of the thermal decomposition of the $Ni(OH)_2$ under linear nonisothermal and isothermal conditions in a stream of wet N_2 with varying $p(H_2O)_{ATM}$ values: (a) 0.8, (b) 3.6, and (c) 9.2 kPa.

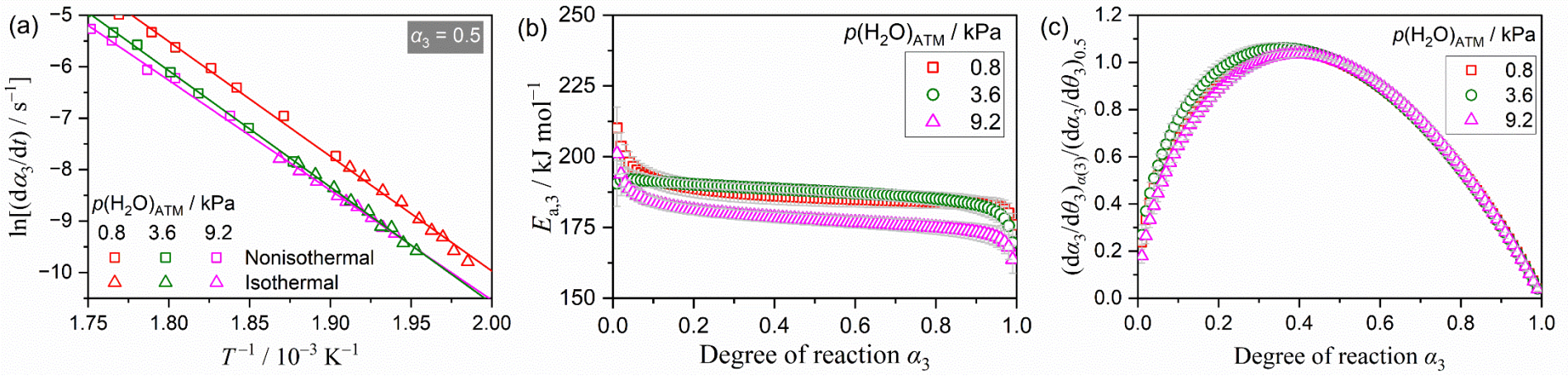

Figure S38. Comparison of the results of formal kinetic analysis for the third reaction step of the thermal decomposition of the $Ni(OH)_2$ at different $p(H_2O)_{ATM}$ values: (a) Friedman plots at α_3 = 0.5, (b) variation of $E_{a,3}$ value as the reaction progressed, and (c) normalized experimental master plot.

Table S9. Kinetic parameters for the third reaction step of the thermal decomposition of $Ni(OH)_2$ at individual $p(H_2O)_{ATM}$ values, determined by the formal kinetic analysis via Friedman plot and experimental master plot methods

$p(H_2O)_{ATM}$ / kPa	$E_{a,3}$ / kJ mol^{-1}, [a]	$\frac{d\alpha_3}{d\theta_3} = A_3 f_3(\alpha_3)$ with $f_3(\alpha_3) = \alpha_3^{m_3}(1-\alpha_3)^{n_3}[-\ln(1-\alpha_3)]^{p_3}$				
		A_3 / s^{-1}	m_3	n_3	p_3	$R^{2,b}$
0.8	186.1 ± 2.2	(4.68 ± 0.02) × 10^{16}	0.94 ± 0.03	0.79 ± 0.01	–0.37 ± 0.03	0.9999
3.6	187.8 ± 2.1	(2.77 ± 0.01) × 10^{15}	0.40 ± 0.03	0.96 ± 0.01	0.11 ± 0.03	0.9999
9.2	177.9 ± 2.6	(3.02 ± 0.01) × 10^{14}	0.59 ± 0.03	0.96 ± 0.01	0.02 ± 0.03	0.9999

[a] Averaged over $0.10 \le \alpha_3 \le 0.90$.
[b] Determination coefficient of the nonlinear least-squares analysis.

S4-4. Extended kinetic analysis of the primary process by considering the effect of $p(H_2O)_{ATM}$

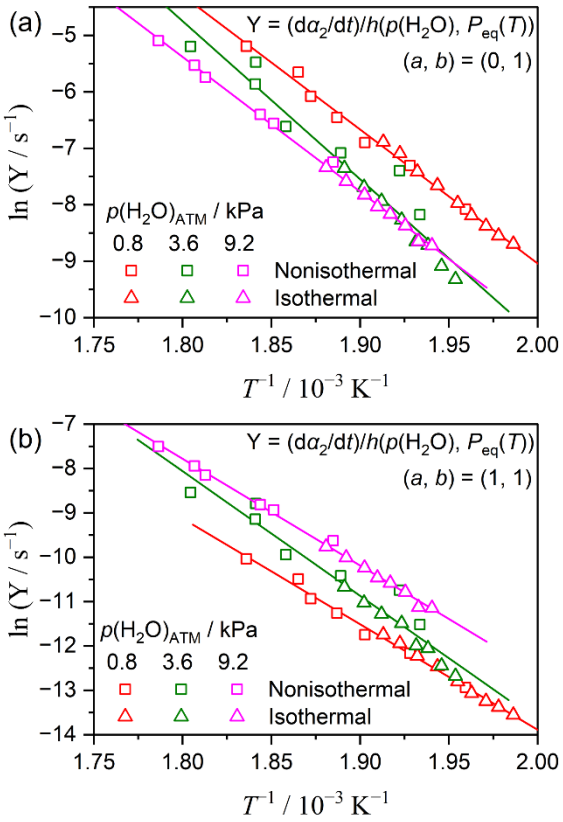

Figure S39. Extended Friedman plots considering the effect of $p(H_2O)_{ATM}$ for the second reaction step at α_2 = 0.5 with specified (a, b) values: (a) (0, 1) and (b) (1, 1).

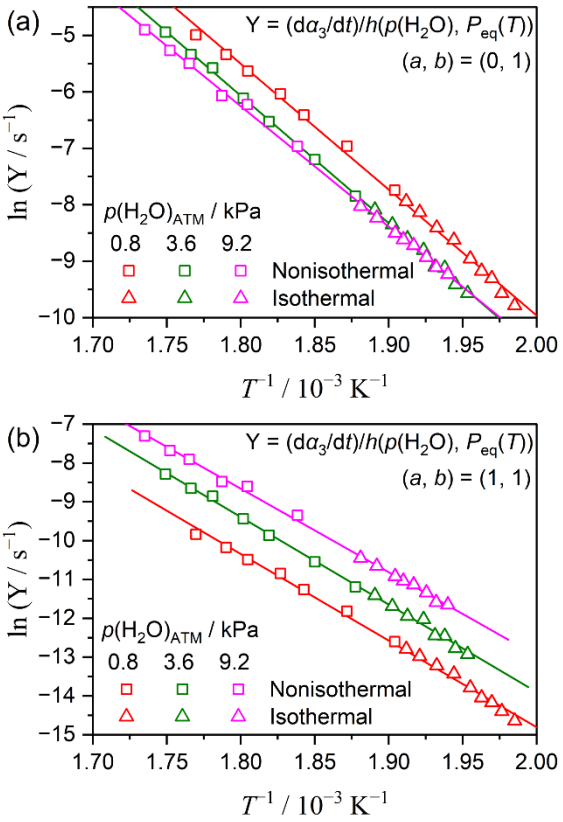

Figure S40. Extended Friedman plots considering the effect of $p(H_2O)_{ATM}$ for the third reaction step at α_3 = 0.5 with specified (a, b) values: (a) (0, 1) and (b) (1, 1).

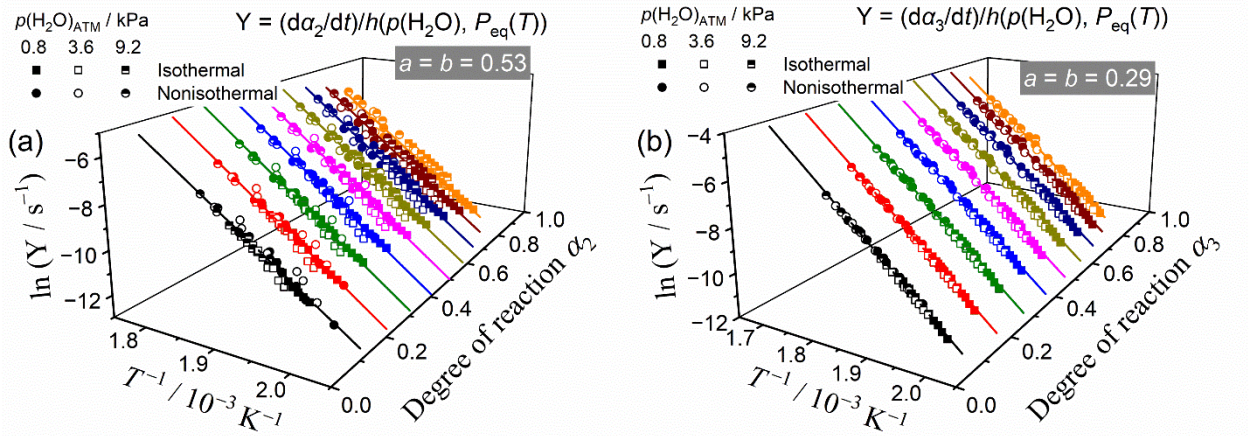

Figure S41. Extended Friedman plots considering the effect of $p(H_2O)_{ATM}$ for the individual reaction steps with optimized a = b values: (a) second reaction step with a = b = 0.53 and (b) third reaction step with a = b = 0.29.

S5. Universal kinetic description considering atmospheric and self-generated water vapor pressures

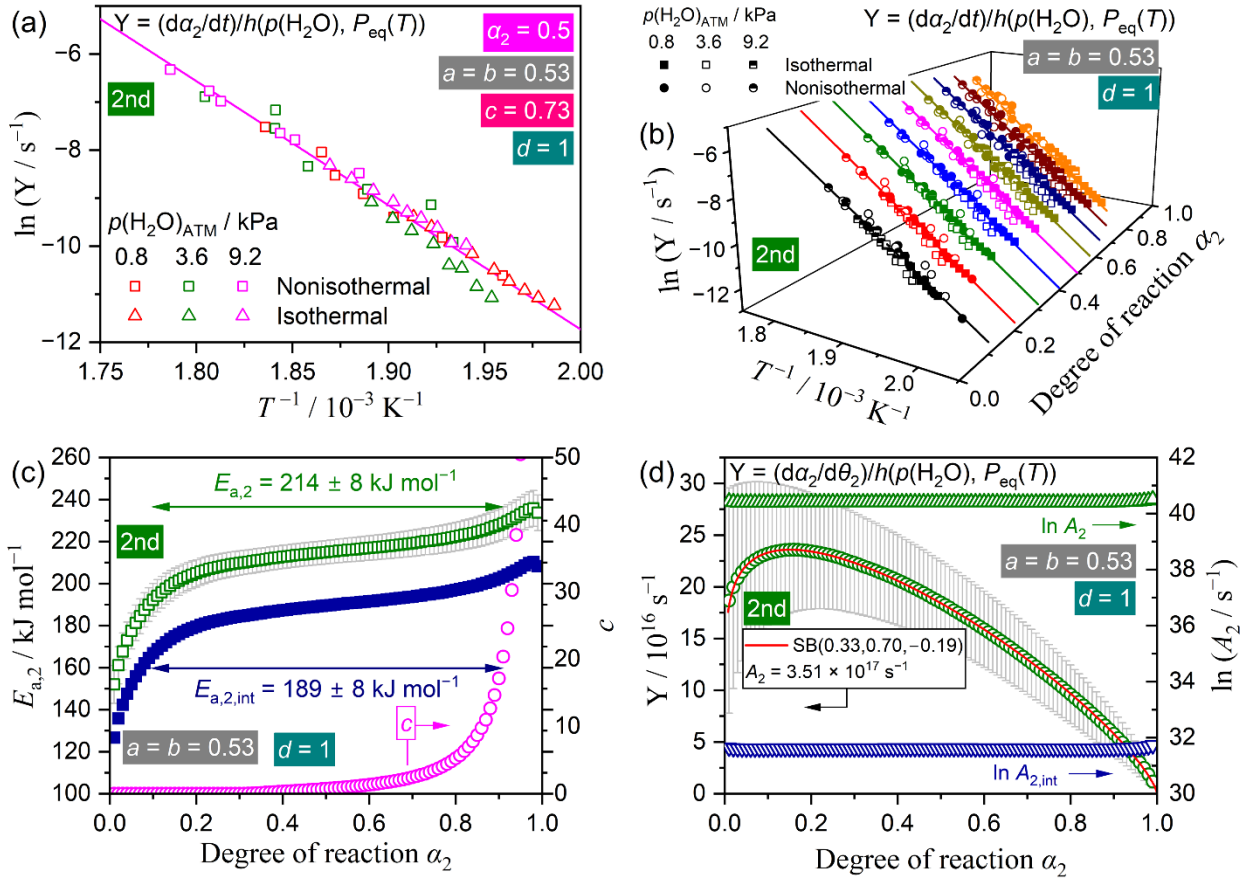

Figure S42. Extended kinetic analysis considering the effect of $p(H_2O)_{SG}$ and $p(H_2O)_{ATM}$ for the second reaction step of the thermal decomposition of $Ni(OH)_2$ in a stream of wet N_2 with the optimized $a = b$ and coefficient (c, d) values: (a) extended Friedman plot with $a = b = 0.53$ and (c, d) = (0.73, 1) at $\alpha_2 = 0.5$, (b) extended Friedman plots at various α_2 values with $a = b = 0.53$ and $d = 1$, while with c value optimized at each α_2, (c) optimized c value and apparent and intrinsic $E_{a,2}$ values at various α_2 values, and (d) extended experimental master plot with the fitting curve using SB(0.33, 0.70, −0.19) and the apparent and intrinsic A_2 values at various α_2 values.

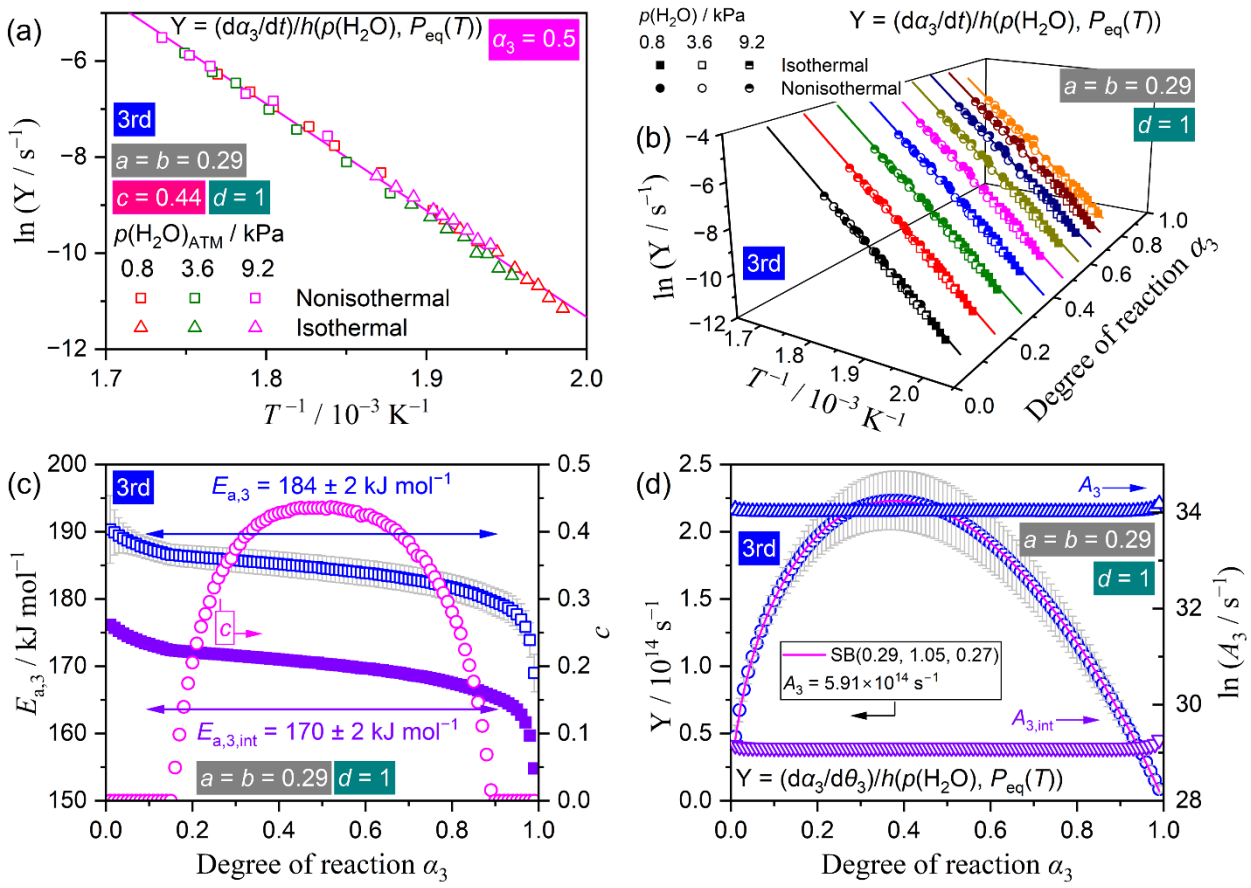

Figure S43. Extended kinetic analysis that incorporated the effect of $p(H_2O)_{SG}$ and $p(H_2O)_{ATM}$ for the third reaction step of the thermal decomposition of $Ni(OH)_2$ in a stream of wet N_2 with the optimized $a = b$ and coefficient (c, d) values: (a) extended Friedman plot with $a = b = 0.29$ and (c, d) = (0.44, 1) at $\alpha_3 = 0.5$, (b) extended Friedman plots at various α_3 values with $a = b = 0.29$ and $d = 1$, while with c value optimized at each α_3, (c) optimized c value and apparent and intrinsic $E_{a,3}$ values at various α_3 values, and (d) extended experimental master plot with the fitting curve using SB(0.29, 1.05, 0.27) and the apparent and intrinsic A_3 values at various α_3 values.

Table S10. Apparent kinetic parameters for the second and third reaction steps of the thermal decomposition of $Ni(OH)_2$ in a stream of wet N_2, determined by considering the effects of $p(H_2O)_{SG}$ and $p(H_2O)_{ATM}$ values, with the optimized $a = b$ and coefficients (c, d)[a], as well as the intrinsic Arrhenius parameters calculated according to eqs. (17) and (18)

Reaction step, i	$a = b$	$E_{a,i}$ / kJ mol^{-1}, [b]	$\frac{(d\alpha_i/d\theta_i)}{h\left(p(H_2O), P_{eq}(T)\right)} = A_i f_i(\alpha_i)$ with $f_i(\alpha_i) = \alpha_i^{m_i}(1-\alpha_i)^{n_i}[-\ln(1-\alpha_i)]^{p_i}$					Intrinsic Arrhenius parameters, [b]	
			A_i / s^{-1}	m_i	n_i	p_i	R^2, [c]	$E_{a,i,int}$ / kJ mol^{-1}	$A_{i,int}$ / s^{-1}
2	0.53	213.9 ± 7.8	(3.51 ± 0.02) × 10^{17}	0.33 ± 0.06	0.70 ± 0.03	–0.19 ± 0.06	0.9998	188.6 ± 7.8	(5.41 ± 0.09) × 10^{13}
3	0.29	184.2 ± 2.0	(5.91 ± 0.02) × 10^{14}	0.29 ± 0.04	1.05 ± 0.02	0.27 ± 0.04	0.9999	170.1 ± 2.0	(4.38 ± 0.10) × 10^{12}

[a] Coefficient c was optimized at individual α_i values, while d was fixed to be unity.
[b] Averaged over $0.10 \leq \alpha_i \leq 0.90$.
[c] Determination coefficient of the nonlinear least-squares analysis.

References

(S1) S. Vyazovkin, A. K. Burnham,; J. M. Criado, L. A. Pérez-Maqueda,; C. Popescu, N. Sbirrazzuoli, *Thermochim. Acta,* **2011**, *520*, 1-19. DOI: 10.1016/j.tca.2011.03.034.
(S2) N. Koga, J. Šesták, P. Simon, Some Fundamental and Historical Aspects of Phenomenological Kinetics in the Solid State Studied by Thermal Analysis. In *Thermal analysis of Micro, Nano- and Non-Crystalline Materials*, J. Šesták, , P. Simon, Eds.; Springer, 2013; pp 1-28.
(S3) H. L. Friedman, *J. Polym. Sci., Part C,* **1964**, *6*, 183-195. DOI: 10.1002/polc.5070060121.
(S4) N.V. Muravyev, A.N. Pivkina, N. Koga, *Molecules,* **2019**, *24*, 2298. DOI: 10.3390/molecules24122298.
(S5) T. Ozawa, *Bull. Chem. Soc. Jpn.,* **1965**, *38*, 1881-1886. DOI: 10.1246/bcsj.38.1881.
(S6) J. Málek, *Thermochim. Acta,* **1992**, *200*, 257-269. DOI: 10.1016/0040-6031(92)85118-f.
(S7) N. Koga, *Thermochim. Acta,* **1995**, *258*, 145-159. DOI: 10.1016/0040-6031(95)02249-2.
(S8) F. J. Gotor, J. M. Criado, J. Malek, N. Koga, *J. Phys. Chem. A,* **2000**, *104*, 10777-10782. DOI: 10.1021/jp0022205.
(S9) J.M. Criado, L.A. Perez-Maqueda, F.J. Gotor, J. Malek, N. Koga, *J. Therm. Anal. Calorim.,* **2003**, *72*, 901-906. DOI: 10.1023/a:1025078501323.
(S10) T. Ozawa, *Thermochim. Acta,* **1986**, *100*, 109-118. DOI: 10.1016/0040-6031(86)87053-8.
(S11) J. Šesták, G. Berggren, *Thermochim. Acta,***1971**, *3*, 1-12. DOI: 10.1016/0040-6031(71)85051-7.
(S12) J. Šesták, *J. Therm. Anal.,* **1990**, *36*, 1997-2007. DOI: 10.1007/bf01914116.
(S13) J. Šesták, *J. Therm. Anal. Calorim.,* **2011**, *110*, 5-16. DOI: 10.1007/s10973-011-2089-1.
(S14) D.D. Wagman, W.H. Evans, V.B. Parker, R.H. Schumm, I. Halow,; S.M. Bailey, K.L. Churney, R.L. Nuttall, *The NBS Tables of Chemical Thermodynamic Properties. Selected Values for Inorganic and C1 and C2 Organic Substances in SI Units*; American Chemical Society, 1982.